



# Anchoring and reactivation of single-site Co–porphyrin over TiO<sub>2</sub> for the efficient photocatalytic CO<sub>2</sub> reduction <sup>☆</sup>



Chao Zhang <sup>a</sup>, Jiwon Yang <sup>a</sup>, Keisuke Hara <sup>a</sup>, Rento Ishii <sup>a</sup>, Hongwei Zhang <sup>a</sup>, Takaomi Itoi <sup>b</sup>, Yasuo Izumi <sup>a,\*</sup>

<sup>a</sup> Department of Chemistry, Graduate School of Science, Chiba University, Yayoi 1-33, Inage-ku, Chiba 263-8522, Japan

<sup>b</sup> Department of Mechanical Engineering, Graduate School of Engineering, Chiba University, Yayoi 1-33, Inage-ku, Chiba 263-8522, Japan

## ARTICLE INFO

### Article history:

Received 22 March 2022

Revised 6 July 2022

Accepted 6 July 2022

Available online 16 July 2022

### Keywords:

CO<sub>2</sub> photoreduction

Cobalt

Porphyrin

TiO<sub>2</sub>

Reactivation

## ABSTRACT

Porphyrin and its derivatives have been often used for electrochemical and photocatalysis combined with first-row transition metals for sustainable applications. Cobalt–tetrakis(4-carboxyphenyl)porphyrin (Co–TCPP) was covalently anchored onto TiO<sub>2</sub>. Under CO<sub>2</sub>, H<sub>2</sub>, and UV–visible light irradiation, Co–TCPP anchored on TiO<sub>2</sub> produced CO at a rate of 2.5 μmol h<sup>−1</sup> (using 100 mg of catalyst and UV–visible light of 118 mW cm<sup>−2</sup>) when the Co–TCPP content was 2.5 wt %; however, the CO formation rate dropped to 0.3 μmol h<sup>−1</sup> (using 100 mg of catalyst and the same intensity of light). The photoactivity drop to 12 % was solved by removing the hydroxy ligands coordinated to the central Co ions through ethanol treatment for 5 min of the Co–TCPP–TiO<sub>2</sub> photocatalysts. This resulted in an increased CO photoformation rate to 7.3 μmol h<sup>−1</sup> (using 100 mg of catalyst and the same intensity of light) because the dispersion of the J- and/or H-aggregates to the isolated Co–TCPP unit proceeded more with ethanol treatment and under UV–visible light. Conversely, to use ethanol as reductant was not effective because it reduced and deactivated Co–TCPP.

© 2022 Elsevier Inc. All rights reserved.

## 1. Introduction

Photocatalytic conversion of CO<sub>2</sub> into renewable energy sources or high value-added compounds using homogeneous or heterogeneous catalysts is a feasible solution to simultaneously address energy shortage and environmental pollution [1–3]. The conversion of CO<sub>2</sub> into methane, methanol, and CO, among others, has been reported using composites of noble metals and semiconductors [4–6], metal complexes [7], and metal–organic frameworks [8]. Among various catalysts, semiconductors, especially TiO<sub>2</sub>, have been extensively studied because of their inexpensive price, stability, and superior photooxidation activity, often combined with noble metal nanoparticles or metal complexes [9].

Metal complexes are usually applied as homogeneous catalysts, allowing precise control of the catalytic properties. Nevertheless, they suffer from quick deactivation within a few hours of photoreaction [10,11]. Accurate molecular design of metal complexes and further appropriate combination with semiconductors enable higher catalytic activity while keeping the robust structure. Although various novel metal complex–semiconductor composites

have been designed and showed high catalytic activities [12–14], the chemical environment around the active single atom site, e.g., the coordination around the active site and the adsorption of reactants, has been rarely studied as well as the time-course monitoring of isotope-labeled <sup>13</sup>C productions from <sup>13</sup>CO<sub>2</sub> under UV–visible light irradiation [4–6].

In this study, detailed active structure of single Co site and the reactivation were intensively studied as the central problems for supported/unsupported molecular photocatalysts [1,12–14]. A cobalt–tetrakis(4-carboxyphenyl)porphyrin (Co–TCPP) complex and a TiO<sub>2</sub> semiconductor were combined to prepare a photocatalyst that exhibits high activity of reducing CO<sub>2</sub> to CO. The site coordination and electronic structure of the active Co sites were monitored via UV–visible absorption spectroscopy and extended X-ray absorption fine structure (EXAFS), and the intermediate surface species during CO<sub>2</sub> reduction were monitored via Fourier transform infrared (FTIR) spectroscopy.

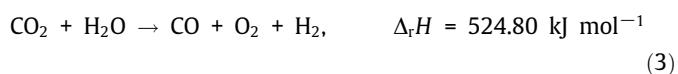
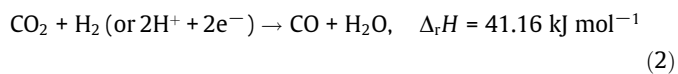
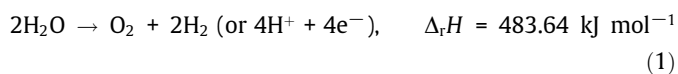
This study mainly evaluated the reaction in Eq. (2) that follows water photooxidation reaction (Eq. (1)) [4–6,15,16]. The efficient photoreduction of CO<sub>2</sub> via Eq. (2) proceeded on a Co–TCPP–TiO<sub>2</sub> composite. Overall reaction of Eq. (3) was also tried using water as reductant. Nevertheless, the rate decreased to 12 % of that using a fresh photocatalyst after 9 h of photoreaction using H<sub>2</sub> as already reported in the literature as a typical weak point of metal–porphyrin electrochemical catalysts [17–20] and photocatalysts

<sup>☆</sup> Dedicated to Takeo Izumi (1936–2022).

\* Corresponding author.

E-mail address: [yizumi@faculty.chiba-u.jp](mailto:yizumi@faculty.chiba-u.jp) (Y. Izumi).

[21–25]. To overcome the drawback, photocatalyst reactivation was attempted and the overall reaction of “artificial photosynthesis” was tested to form CO as indicated in Eq. (3), which is the summation of Eqs. (1) and (2). Assuming a system of constant pressure:



## 2. Experimental

### 2.1. Photocatalyst synthesis

4-Formylbenzoic acid (purity > 97 %), pyrrole (purity > 98 %), cobalt(II) chloride hexahydrate ( $\text{CoCl}_2 \cdot 6\text{H}_2\text{O}$ , purity > 98 %), and *N,N*-dimethylformamide (DMF, purity > 99.8 %) were purchased from Sigma-Aldrich, St. Louis, MO, USA. Propionic acid, methanol (purity > 99.8 %), and ethanol (purity > 99.5 %) were purchased from Wako Pure Chemical, Japan.  $\text{TiO}_2$  [major anatase phase, purity > 93.4 %, mean particle size 7.4 nm, specific surface area (SA)  $308 \text{ m}^2 \text{ g}^{-1}$ ; JRC-TIO-14, Catalysis Society of Japan (CSJ)] and  $\text{TiO}_2$  (rutile phase, chemical purity > 99 %, mean particle size 15 nm, specific SA  $110 \text{ m}^2 \text{ g}^{-1}$ ; JRC-TIO-6, CSJ) were provided by Ishihara Sangyo Kaisha, Ltd., Osaka, Japan and Sakai Chemical Industry Co., Ltd, Japan, respectively. JRC-TIO-14 was mostly used in this study and JRC-TIO-6 was tested as a reference.

H-TCPP compound was synthesized via a previously reported procedure [26]. 4-Formylbenzoic acid (6.08 g, 40.5 mmol) was dissolved in propionic acid (150 mL), and pyrrole (2.9 mL, 40.5 mmol) was added dropwise within 20 s. The mixed solution was ultrasonicated (430 W, 38 kHz) for 10 min and was refluxed at 423 K for 2 h. Then, the solution was added to methanol (200 mL) and stirred at a rate of 2,000 rotations per minute (rpm) for 30 min at 273 K, resulting in a dark purple precipitate. The precipitate was filtrated using a polytetrafluoroethylene (PTFE)-based membrane filter (pore size 0.1  $\mu\text{m}$ ; Omnipore JWVP04700, Millipore, Burlington, MA, USA) and washed with methanol (200 mL) and deionized water (100 mL,  $<0.055 \mu\text{S cm}^{-1}$  supplied by an RFU424TA system, Advantec, Tokyo, Japan). After drying in vacuum at 353 K for 6 h, H-TCPP was obtained as a purple powder with a yield of 15 %.

The as-prepared H-TCPP (0.24 g, the molecular weight 790.77, 0.30 mmol) and  $\text{CoCl}_2 \cdot 6\text{H}_2\text{O}$  (0.36 g, 1.5 mmol) were dissolved in DMF (15 mL), followed by ultrasonication for 10 min. Then, the mixed solution was refluxed at 433 K for 5 h. The red precipitate was washed with deionized water three times (60 mL each) and dried in vacuum at 333 K for 5 h. The obtained sample was brick color powder with a yield of 99.9 % and was denoted as Co-TCPP (molecular weight 847.69).

$\text{TiO}_2$  (0.5 g) was suspended in ethanol (60 mL) with stirring at 700 rpm for 10 min. Then, Co-TCPP was added into the suspension and was kept stirred at 700 rpm for 4 h. The precipitate was filtered using JWVP04700, washed with ethanol (20 mL), and dried in vacuum at 298 K for 3 h. The Co-TCPP content in the composite was varied at 1.0, 2.5, 5.0, and 7.5 wt %. The filtrate was almost colorless demonstrating that most of the introduced Co-TCPP was supported on  $\text{TiO}_2$ . The obtained powder was denoted as Co-TCPP- $\text{TiO}_2$ . As the Co-TCPP content in the catalyst was increased, the color of the catalyst changed from light orange (1.0 wt %), to dark orange (2.5 wt %), and then finally to deep orange (7.5 wt %).

H-TCPP (2.5 wt %)- $\text{TiO}_2$  was prepared using a similar procedure to that of Co-TCPP- $\text{TiO}_2$ . Similarly, most of H-TCPP was supported on  $\text{TiO}_2$  after the filtration and washing. The color of obtained powder was purple.

### 2.2. Photocatalytic $\text{CO}_2$ reduction

The composite photocatalyst (0.100 g) was placed in a quartz photoreactor (bottom plate area  $23.8 \text{ cm}^2$ , volume 45.5 mL) [1,15,27] connected to a Pyrex glass circulation system (206.1 mL) and evacuated using rotary and diffusion pumps ( $10^{-6}$  Pa). The photocatalyst was treated in vacuum for 1 h. Then, 2.7 kPa of  $^{13}\text{CO}_2$  ( $^{13}\text{C}$  99.0 %,  $^{17}\text{O}$  0.1 %,  $^{18}\text{O}$  0.7 %, chemical purity > 99.9 %; Cambridge Isotope Laboratories, Inc., Tewksbury, MA, USA) and 20.7 kPa of  $\text{H}_2$  (purity > 99.99 %) were introduced. The photocatalyst was irradiated with UV-visible light upward from a 500 W xenon arc lamp (Model OPM2-502; Ushio, Inc., Tokyo, Japan). The distance between the light exit and the sample was 20 mm. The maximum temperature reached under the light irradiation conditions was 328 K [1,15,27]. The light intensity distribution of the xenon (Xe) arc lamp on wavelength was measured using a spectroradiometer (Model USR45DA, Ushio, Inc., Tokyo, Japan) at a distance of 20 mm from the UV-visible light source, and the light intensity at the center of the photocatalyst was measured as  $118 \text{ mW cm}^{-2}$ . Control photocatalytic tests were performed in a similar way using H-TCPP (2.5 wt %)- $\text{TiO}_2$ , Co-TCPP, or  $\text{TiO}_2$  (0.100 g each). A reaction using  $^{13}\text{CO}_2$  (2.7 kPa) and  $\text{H}_2\text{O}$  (1.7 kPa) was also performed under similar conditions.

In-profile kinetic data were collected as a function of the light excitation wavelength by inserting a sharp-cut filter (thickness 2.5 mm; Hoya, Tokyo, Japan) at the exit of a lamp house. Model UV32 (wavelength  $\lambda > 320 \text{ nm}$ ), U330 (245 nm  $< \lambda < 386 \text{ nm}$ , and  $\lambda > 686 \text{ nm}$ ), and L38 ( $\lambda > 380 \text{ nm}$ ) filters were used to pass light of specific wavelength. The absorbance of filters was noted in Supplementary materials [S1–S3]. Reactivation of the used photocatalysts was tried for Co-TCPP (2.5 wt %)- $\text{TiO}_2$  that was used for a photocatalytic test for 48 h under  $\text{H}_2$  (20.7 kPa, 21 h),  $\text{O}_2$  (9.7 kPa, 21 h), or ethanol (2.7 kPa, 5 min) all under the irradiation of UV-visible light.

The analytical conditions of online gas chromatography (GC)-mass spectrometry (MS) measurements were described in detail elsewhere [4–6]. Briefly, a packed column of 13X-S molecular sieves (length 3 m, internal diameter 3 mm; GL Sciences, Inc., Tokyo, Japan) for the  $\text{CO}_2$  photoreduction tests or polyethylene glycol 6000/Flusin P support column (length 3 m, internal diameter 3 mm; GL Sciences, Inc., Tokyo, Japan) for the  $\text{CO}_2$  exchange tests was applied in GC-MS (Model JMS-Q1050GC, JEOL, Tokyo, Japan) using helium (purity > 99.99995 %) as the carrier gas.

### 2.3. Characterizations

UV-visible absorption spectra were obtained in diffuse-reflectance (DR) mode for solid samples and in transmission mode for samples dissolved in ethanol in the wavelength range from 200 to 800 nm using a spectrophotometer (Model V-650; JASCO, Tokyo, Japan) equipped with  $\text{D}_2$  and halogen lamps of wavelength below and above 340 nm, respectively, and with an integrated ISV-469 sphere in DR mode. A formed PTFE plate was used as a reference in diffuse-reflectance mode, and the data were transformed into corresponding absorbance spectra using the Kubelka-Munk function [15,27].

The surface species on the catalysts were monitored using a single-beam FTIR instrument (Model FT/IR-4200; JASCO, Tokyo, Japan) equipped with a mercury-cadmium-tellurium-M detector at a temperature of 77.4 K. A self-supporting disk (diameter  $\Phi = 20 \text{ mm}$ ) of Co-TCPP (2.5 wt %)- $\text{TiO}_2$  (10 mg) diluted with

TiO<sub>2</sub> (60 mg) was placed in a quartz photoreaction IR cell equipped with NaCl windows on both sides. The cell was connected to a Pyrex glass circulation system also connected to GC–MS to enable simultaneous monitoring of the surface species and products. The sample disk was treated in vacuum for 1 h before the measurements.

FTIR measurements were performed at 298 K in a wave number range of 4000–650 cm<sup>-1</sup>. The sample (Co–TCPP–TiO<sub>2</sub> or TiO<sub>2</sub>) disk was irradiated with UV–visible light from a 500 W Xe arc lamp via a Y-shaped quartz fiber light guide (40-cm-long fiber and 80-cm-long branches, Model 1.2S15-1000F-1Q7-SP-RX; Optel, Tokyo, Japan). The distance between the fiber light exit and sample disk was 46 mm. The light intensity at the sample center was 150 mW cm<sup>-2</sup>. The energy resolution of the spectrometer was 1 cm<sup>-1</sup>, and the data accumulation included 128 scans (~2 s per scan). The spectrum of the fresh sample treated in vacuum was used as a background for subtraction from the spectra during reaction tests.

The binding between Co–TCPP and TiO<sub>2</sub> was studied using DR FTIR using KBr pellets. The data were subtracted by the data of TiO<sub>2</sub> to elucidate the change in Co–TCPP before and after combined with TiO<sub>2</sub>.

Transmission electron microscopy (TEM) was performed using JEM-2100F (JEOL, Tokyo, Japan) equipped with a field emission gun (acceleration voltage of 200 kV) at the Center for Analytical Instrumentation. The samples were mounted on a Cu mesh (250 meshes per inch) coated with carbon and a copolymer film of poly(vinyl alcohol) and formaldehyde (Formvar, Monsanto, St. Louis, MO, USA). High-angle annular dark-field scanning TEM and high-resolution (HR) TEM images were observed. The chemical compositions and elemental distributions were analyzed using energy-dispersive spectra with a Si (Li) detector equipped in JEM-2100F.

Co K-edge X-ray absorption fine structure (XAFS) measurements and the spectral analyses were described in detail elsewhere [4–6]. In brief, the spectra were measured at 298 K in the transmission mode at the Photon Factory, High Energy Accelerator Research Organization (Tsukuba, Japan) on a 9C beamline equipped with a Si (1 1 1) double-crystal monochromator, an Rh-coated focusing bent cylindrical mirror, and a piezotransducer. The Co K-edge absorption energy was calibrated at 7709.54 eV [28] using the X-ray spectrum of Co metal (thickness 10 μm).

A Co–TCPP (25 wt %)-TiO<sub>2</sub> (Φ = 10 mm, 30 mg) disk was set in a Pyrex glass reactor equipped with a Kapton film (thickness 50 μm; Dupont, Wilmington, DE, USA) on both sides for X-ray transmission using 2.7 kPa of CO<sub>2</sub>, 20.7 kPa of H<sub>2</sub>, and UV–visible light from a Xe arc lamp via branches of a quartz fiber light guide 1.2S15-1000F-1Q7-SP-RX. The samples were irradiated under UV–visible light on the beamline. The distance between the light exit of the quartz fiber light guide and the sample was 50 mm. In comparison, a sample under argon (Ar) was also measured under similar conditions.

The Co K-edge XAFS spectra for Co–TCPP (2.5 wt %)-TiO<sub>2</sub> (170 mg) sample in a glass cell equipped with Kapton windows was measured in fluorescence detection mode using Lytle detector [29].

The obtained Co K-edge EXAFS data were analyzed using an XDAP software package [30]. Multiple-shell curve-fit analyses were performed on the Fourier-filtered angular photoelectron wave number *k*<sup>3</sup>-weighted EXAFS data in *k*- and interatomic distance *R*-space on the basis of the plane-wave approximation for amplitude *A<sub>i</sub>(k)*, coordination number *N<sub>i</sub>*, backscattering amplitude *f<sub>i</sub>*, Debye–Waller factor *σ<sub>i</sub>*, and mean free photoelectron path *λ* for shell *i*:

$$A_i(k) = \frac{N_i}{kR_i^2} |f_i(k)| \exp \left[ -2 \left( \sigma_i k^2 + \frac{R_i}{\lambda} \right) \right], \quad i = \text{Co} \quad (4)$$

The empirical parameters were extracted from the EXAFS data for the Co metal (thickness 10 μm), CoO powder, and the Co–TCPP powder. The *R* and *N* values of the Co–Co interatomic pair in Co metal (hexagonal closed packed) were set to 0.2502 nm and 12, respectively [31]. Those values of the Co–O interatomic pair in CoO powder (cubic) were set to 0.2131 nm and 6, respectively [32]. Those values of the Co–N interatomic pair in Co–TCPP crystal were set to 0.196 nm and 4, respectively [13]. The many-body reduction factor *S<sub>0</sub>*<sup>2</sup> was assumed to be identical for both the sample and reference.

## 2.4. Calculations

Density functional theory (DFT) calculations were performed using Gaussian 09 W [33] through a mixed basis set of lan12DZ for the Co metal and 6–31 + G(d) for the other elements (H, C, N, and O) and the hybrid-GGA functional (U)B3LYP. The most stable molecular structure and energy of each orbital were obtained on the basis of structural optimization. The band gap value was evaluated on the basis of the difference between the highest occupied molecular orbital (HOMO) and lowest unoccupied molecular orbital (LUMO).

## 3. Results and discussion

### 3.1. Photocatalytic CO<sub>2</sub> reduction using H<sub>2</sub>

The photocatalytic tests were performed using Co–TCPP–TiO<sub>2</sub> composites, <sup>13</sup>CO<sub>2</sub>, H<sub>2</sub>, and UV–visible light irradiation instead of typical sacrificial reagents, e.g., triethanolamine [7,34]. Among the Co–TCPP (1.0–7.5 wt %)-TiO<sub>2</sub> photocatalysts, the maximum initial <sup>13</sup>CO formation was obtained using Co–TCPP (2.5 wt %)-TiO<sub>2</sub> at a rate of 17 μmol h<sup>-1</sup> g<sub>cat</sub><sup>-1</sup> (1.7 μmol h<sup>-1</sup>; Fig. 1A). For convenience, the value is noted as the rate per catalyst weight. However, the photocatalytic test conditions were commonly using 100 mg of catalyst and UV–visible light of 118 mW cm<sup>-2</sup>. Although the linearity is not always guaranteed between catalyst amount and photocatalytic formation rate, especially for catalysis at the interface of liquid (reactants)–solid (catalyst), we use the unit of μmol h<sup>-1</sup> g<sub>cat</sub><sup>-1</sup> in this paper based on the linearity between 20 and 100 mg of photocatalyst (Fig. S1) [15,27]. <sup>12</sup>CO was also constantly formed at a rate of 7.1 μmol h<sup>-1</sup> g<sub>cat</sub><sup>-1</sup> (Fig. 1C). The total CO formation rate was 25 μmol h<sup>-1</sup> g<sub>cat</sub><sup>-1</sup>, and <sup>12</sup>C ratio in the initially formed CO was 29 % (entry a in Table 1), suggesting that the preadsorbed <sup>12</sup>CO<sub>2</sub> from the air on the photocatalyst remained and was photo-reduced to <sup>12</sup>CO. The formed <sup>13</sup>CO/<sup>12</sup>CO ratio was essentially constant throughout the photocatalytic test (Fig. 1C), while the <sup>12</sup>CO<sub>2</sub> ratio in gas phase during <sup>13</sup>CO<sub>2</sub> (0.67 kPa) photoexchange reaction due to partial decomposition of Co–TCPP was 16 % at the maximum (Fig. S2, Supplementary materials), and the <sup>12</sup>CO<sub>2</sub> ratio during CO<sub>2</sub> (2.7 kPa) photoreduction tests using H<sub>2</sub> was less. Thus, the products were preferably formed via the <sup>12</sup>CO<sub>2</sub>-preadsorbed site and <sup>13</sup>CO<sub>2</sub>- and <sup>12</sup>CO<sub>2</sub>-derived species were equilibrated during CO<sub>2</sub> photoreduction [4–6].

The <sup>13</sup>CO formation rate increased by 9.1 times in Co–TCPP (2.5 wt %)-TiO<sub>2</sub> compared with Co–TCPP (1.0 wt %)-TiO<sub>2</sub> (Fig. 1A, entries a and b in Table S1), suggesting a synergistic reaction mechanism by the combination of Co–TCPP with TiO<sub>2</sub> surface. Conversely, the <sup>13</sup>CO formation rate gradually decreased when the Co–TCPP content increased to >2.5 wt % (Fig. 1A, entries b–e in Table S1).

The <sup>12</sup>CO ratio for all the total CO formations rapidly increased as the photocatalytic activity decreased (Tables 1 and S1) because preadsorbed <sup>12</sup>CO<sub>2</sub> from the air preferably adsorbed on the Co–TCPP active site when the overall photocatalytic CO<sub>2</sub> reduction rate

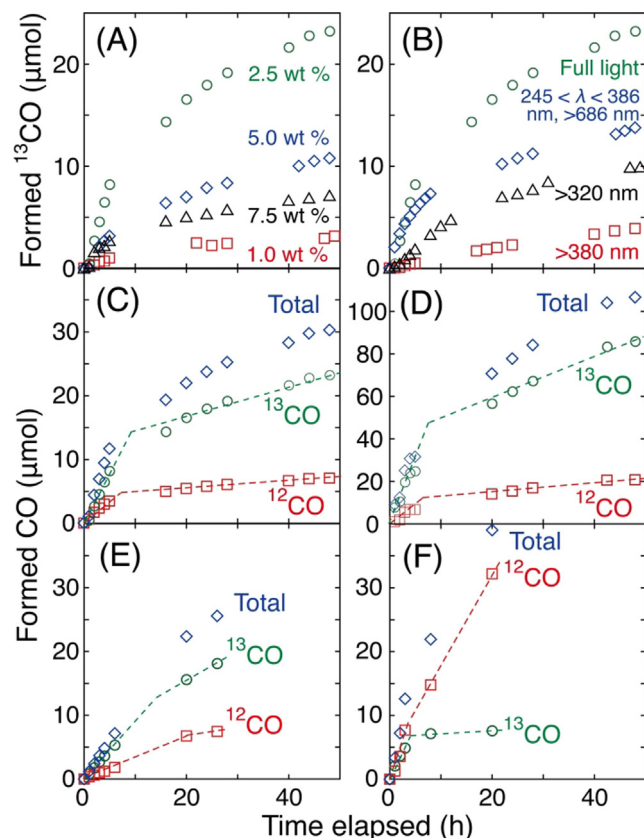


**Fig. 1.** Time-course formation of photocatalytic (A–F)  $^{13}\text{CO}$  and (C–F)  $^{12}\text{CO}$  and the sum of  $^{13}\text{CO}$  and  $^{12}\text{CO}$  (C–F) during exposure to  $^{13}\text{CO}_2$  (2.7 kPa) and  $\text{H}_2$  (20.7 kPa) using (A) Co-TCPP (1.0, 2.5, 5.0, and 7.5 wt %)- $\text{TiO}_2$  under UV-visible light; (B) Co-TCPP (2.5 wt %)- $\text{TiO}_2$  irradiated under full light and filtered light of  $\lambda > 320$  nm;  $\lambda > 380$  nm; and  $245 \text{ nm} < \lambda < 386 \text{ nm}$  and  $\lambda > 686 \text{ nm}$ ; and (C) Co-TCPP (2.5 wt %)- $\text{TiO}_2$  under UV-visible light. (D, E) Co-TCPP (2.5 wt %)- $\text{TiO}_2$  used for the test in panel C was treated with ethanol (2.7 kPa) for 5 min and irradiated under UV-visible light under (D)  $^{13}\text{CO}_2$  (2.7 kPa) and  $\text{H}_2$  (20.7 kPa) and (E)  $^{13}\text{CO}_2$  (2.7 kPa). (F) Time-course formation of photocatalytic  $^{13}\text{CO}$  and  $^{12}\text{CO}$  and the sum of  $^{13}\text{CO}$  and  $^{12}\text{CO}$  during exposure to  $^{13}\text{CO}_2$  (2.7 kPa) and  $\text{C}_2\text{H}_5\text{OH}$  (2.7 kPa) using Co-TCPP (2.5 wt %)- $\text{TiO}_2$  under UV-visible light. Photocatalyst amount was 100 mg and the UV-visible light intensity was  $118 \text{ mW cm}^{-2}$ .

became slower. In contrast, partial decomposition rate of Co-TCPP irradiated under UV-visible light should be always constant in 10 h of reaction (Fig. S2). The maximum of CO formation rate was at much lower loading of Co-TCPP (2.5 wt %) for clarity compared to the total area of Co-TCPP molecules (Scheme 1,  $\sim 1 \text{ nm}^2$  per molecule; 30 wt %) to cover the  $\text{TiO}_2$  surface, clearly neglecting flat orientation of Co-TCPP to the  $\text{TiO}_2$  surface and suggesting a specific interaction of Co-TCPP with  $\text{TiO}_2$  and also significant blocking

**Table 1**

Initial CO formation rates during the first 5 h of reaction using Co-TCPP (2.5 wt %)- $\text{TiO}_2$ , H-TCPP (2.5 wt %)- $\text{TiO}_2$ , Co-TCPP, and  $\text{TiO}_2$  (100 mg each) under  $^{13}\text{CO}_2$  (2.7 kPa),  $\text{H}_2$  (20.7 kPa),  $\text{H}_2\text{O}$  (1.7 kPa), and UV-visible light irradiation. The UV-visible light intensity was  $118 \text{ mW cm}^{-2}$ .

Entry	Catalyst	Reactant	Irradiated light	Formation rate ( $\mu\text{mol h}^{-1} \text{g}_{\text{cat}}^{-1}$ )				$^{12}\text{CO}$ ratio (mol %)
				$^{13}\text{CO}$	$^{12}\text{CO}$	$\text{O}_2$	$\Sigma \text{CO}$	
a	Co-TCPP (2.5 wt %)- $\text{TiO}_2$	$^{13}\text{CO}_2$ and $\text{H}_2$	UV-visible	17	7.1	–	25	29
a'			$245 \text{ nm} < \lambda < 386 \text{ nm}$ , $\lambda > 686 \text{ nm}$	11	3.6	–	15	25
a''			$\lambda > 320 \text{ nm}$	3.8	1.1	–	4.8	22
a'''			$\lambda > 380 \text{ nm}$	1.1	<0.002	–	1.1	<0.19
a''''		$^{13}\text{CO}_2$ and $\text{H}_2\text{O}$	UV-visible	1.8	4.9	<0.005	6.6	74
b	H-TCPP (2.5 wt %)- $\text{TiO}_2$	$^{13}\text{CO}_2$ and $\text{H}_2$		0.022	0.82	–	0.84	97
c	Co-TCPP			<0.0014	0.38	–	0.38	>99
d	$\text{TiO}_2$			<0.0014	<0.002	–	<0.003	–

effects of light by Co-TCPP. The aggregation of porphyrin resulted in lower photocatalytic activity [35,36].

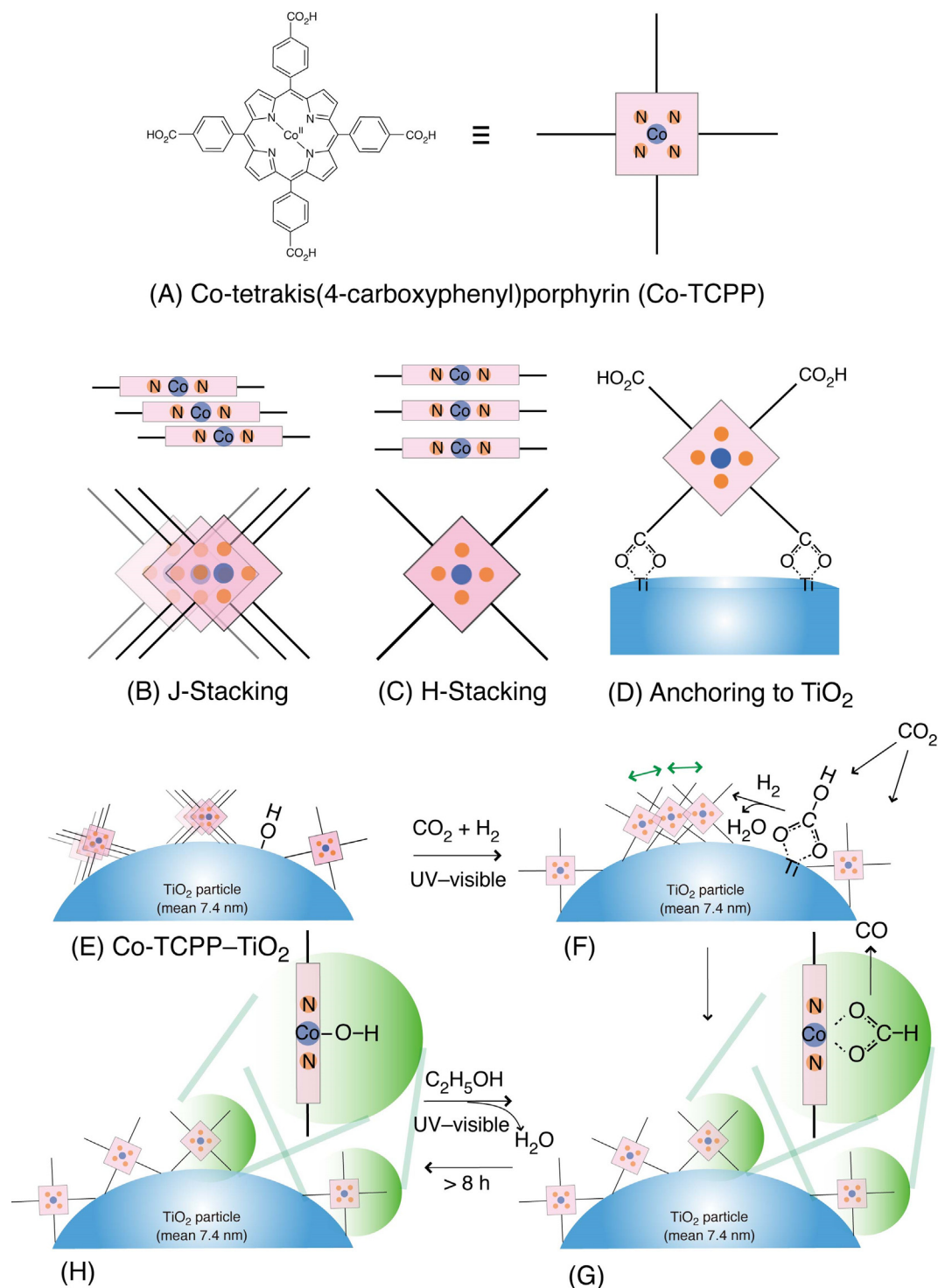
Next, the dependence on light wavelength was tested for the most active Co-TCPP (2.5 wt %)- $\text{TiO}_2$  (Fig. 1B). Under light irradiation of  $245 \text{ nm} < \lambda < 386 \text{ nm}$  and  $\lambda > 686 \text{ nm}$ , i.e., UV and mostly IR light, the  $^{13}\text{CO}$  formation rate moderately decreased to 64 % of that under full UV-visible light irradiation (entries a and a' in Table 1). The  $^{13}\text{CO}$  formation rate under light irradiation of  $\lambda > 320 \text{ nm}$  further decreased to 22 % of that under full light (entry a'' in Table 1). Then, the  $^{13}\text{CO}$  formation rate under light irradiation of  $\lambda > 380 \text{ nm}$ , i.e., visible and IR light, decreased to only 6.1 % of that under full light irradiation (entry a''' in Table 1) because the band gap of anatase-phase  $\text{TiO}_2$  can be excited by light with  $\lambda < 387 \text{ nm}$  [16] and almost all the effective light was filtered ( $\lambda > 380 \text{ nm}$ ). Hence, the UV light with  $\lambda < 380 \text{ nm}$  was essential to  $^{13}\text{CO}_2$  photoreduction using Co-TCPP- $\text{TiO}_2$  (Scheme 2A). Based on the result and also the fact that one third of UV light was absorbed in Co-TCPP- $\text{TiO}_2$  sample, the quantum yield for the highest  $^{13}\text{CO}$  formation rate in this paper ( $63 \mu\text{mol h}^{-1} \text{g}_{\text{cat}}^{-1}$ , Table 2g) was 1.6 % [4,15,16,27].

On the anode of dye-sensitized solar cells, metal complexes and/or dye molecules provide photoexcited electrons to the conduction band (CB) of semiconductors, e.g.,  $\text{TiO}_2$ , and the electrons are transferred to the cathode [34,37]. As the effects of band gap excitation of  $\text{TiO}_2$  on photocatalytic  $\text{CO}_2$  reduction into CO on photocatalysis was predominant based on the critical dependence of CO formation rate on the wavelength of excitation light (Table 1a, a', a'', a'''), two possibilities existed. One is electron flow from CB of  $\text{TiO}_2$  into Co-TCPP and subsequent HOMO-LUMO excitation resulted in  $\text{CO}_2$  reduction (Scheme 2A). The excited electrons in Co-TCPP should be used for photoreduction of  $\text{CO}_2$ , and photoexcited electrons at CB in  $\text{TiO}_2$  compensate the holes in HOMO of Co-TCPP.

The other possibility is  $\text{CO}_2$  reduction by the electrons from CB of  $\text{TiO}_2$ , electron flow from LUMO of Co-TCPP to  $\text{TiO}_2$ , hole flow from valence band (VB) of  $\text{TiO}_2$  to HOMO/HOMO-1 of Co-TCPP, and  $\text{H}_2$  oxidation at Co-TCPP (Scheme 2A). The second scenario is difficult to explain the oxygen source at Co-TCPP, critical CO formation rate dependence on the ratio of Co-TCPP (Table S1), and preferable  $\text{CO}_2$  adsorption on Co site (see 3.6 XAFS section). Thus, we propose the first scenario. The activation of  $\text{H}_2$  would proceed via hole injection to hydrogen at the interface between Co-TCPP and  $\text{TiO}_2$  and the resultant proton combines with hydroxy species on  $\text{TiO}_2$  (see 3.4 FTIR section; Scheme 2A).

Using H-TCPP (2.5 wt %)- $\text{TiO}_2$  that is free from  $\text{Co}^{2+}$  ions, the  $^{13}\text{CO}$  formation rate was only  $0.022 \mu\text{mol h}^{-1} \text{g}_{\text{cat}}^{-1}$  (entry b in Table 1), whereas  $^{13}\text{CO}$  was not detected above the detection limit of GC-MS using Co-TCPP or  $\text{TiO}_2$  (entries c and d in Table 1), demonstrating that the composite of Co-TCPP and  $\text{TiO}_2$  was essential for the photocatalytic formation of  $^{13}\text{CO}$ .

Critically, it can be observed from the time-course trend that there is an initial quick formation of CO and decelerated formation

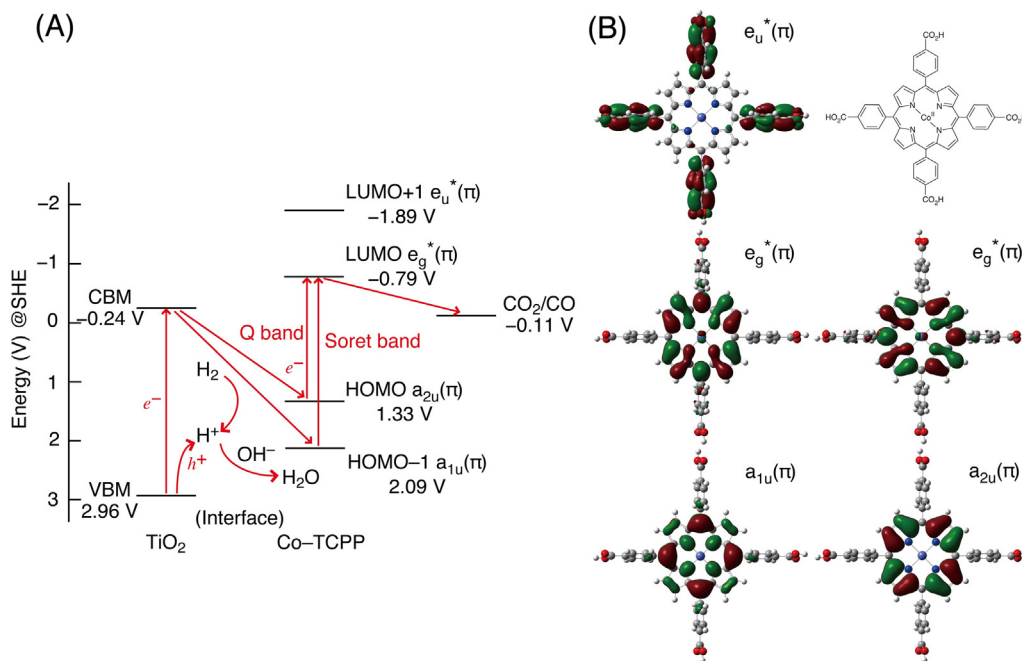


**Scheme 1.** Synthesis, impregnation on TiO<sub>2</sub>, and transformation under CO<sub>2</sub>, H<sub>2</sub>, and UV-visible light of the Co-TCPP-TiO<sub>2</sub> composites.

of CO at 7–9 h of reaction for all the Co-TCPP-TiO<sub>2</sub> photocatalysts (Co-TCPP 1.0–7.5 wt %, Fig. 1A). Using the Co-TCPP (2.5 wt %)-TiO<sub>2</sub> photocatalyst, the initial <sup>13</sup>CO formation rate of 17 μmol h<sup>-1</sup> g<sub>cat</sub><sup>-1</sup> decreased to 12 % (2.3 μmol h<sup>-1</sup> g<sub>cat</sub><sup>-1</sup>) after 9 h of photoreaction (entries a and b in Table 2). Analogously, the initial <sup>12</sup>CO formation rate of 7.1 μmol h<sup>-1</sup> g<sub>cat</sub><sup>-1</sup> decreased to 8.8 % (0.63 μmol h<sup>-1</sup> g<sub>cat</sub><sup>-1</sup>) after 7 h of photoreaction. We tested the reactivation of used Co-TCPP (2.5 wt %)-TiO<sub>2</sub> at the end of this article.

### 3.2. Photocatalytic CO<sub>2</sub> reduction using H<sub>2</sub>O

CO<sub>2</sub> photoreduction tests were also performed using Co-TCPP (2.5 wt %)-TiO<sub>2</sub> under <sup>13</sup>CO<sub>2</sub>, moisture, and UV-visible light irradiation (Fig. S3A). Good CO formation rate of 6.6 μmol h<sup>-1</sup> g<sub>cat</sub><sup>-1</sup> (entry a<sup>\*\*\*</sup> in Table 1) was confirmed as a part of reaction in Eq. (3), and the rate was lower by 27 % compared with that using <sup>13</sup>CO<sub>2</sub> and H<sub>2</sub> (entry a in Table 1, Eq. (2)). Nevertheless, the <sup>12</sup>CO ratio was



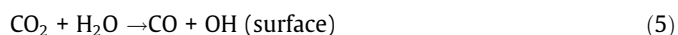
**Scheme 2.** Frontier energy levels for the Co-TCPP–TiO<sub>2</sub> composites and orbital distribution of LUMO + 1, LUMO, HOMO, and HOMO – 1 [38,39].

**Table 2**

Initial and deactivated CO formation rates during the first 5 h of reaction using fresh Co-TCPP (2.5 wt %)-TiO<sub>2</sub> (100 mg) under <sup>13</sup>CO<sub>2</sub> (2.3 kPa), H<sub>2</sub> (21.7 kPa), and UV-visible light irradiation (a, b), under <sup>13</sup>CO<sub>2</sub> (2.3 kPa), C<sub>2</sub>H<sub>5</sub>OH (2.7 kPa), and UV-visible light irradiation (c, d), and reactivated rates (e–l) under similar conditions to entries a (e–j) and under <sup>13</sup>CO<sub>2</sub> (2.3 kPa) and UV-visible light irradiation (k, l) after treatment with H<sub>2</sub> (20.7 kPa; e, f), O<sub>2</sub> (9.7 kPa; g, h), ethanol (2.7 kPa; i–l), and UV-visible light. The UV-visible light intensity was 118 mW cm<sup>-2</sup>.

Entry	Test no.	Reactants	Time-course period	Formation rate (μmol h <sup>-1</sup> g <sub>cat</sub> <sup>-1</sup> )			<sup>12</sup> CO ratio (mol %)
				<sup>13</sup> CO	<sup>12</sup> CO	ΣCO	
a	First test	<sup>13</sup> CO <sub>2</sub> + H <sub>2</sub>	1–7 h of reaction	17	7.1	25	29
b			15–48 h of reaction	2.3	0.63	3.0	21
c		<sup>13</sup> CO <sub>2</sub> + C <sub>2</sub> H <sub>5</sub> OH	1–3 h of reaction	16	26	42	61
d			3–20 h of reaction	1.5	15	16	90
e	Regeneration test (H <sub>2</sub> )	<sup>13</sup> CO <sub>2</sub> + H <sub>2</sub>	1–3 h of reaction	2.3	<0.002	2.3	<0.085
f			15–48 h of reaction	2.3	0.044	2.4	1.8
g	Regeneration test (O <sub>2</sub> )		1–3 h of reaction	<0.0014	<0.002	<0.003	–
h			15–48 h of reaction	<0.0014	0.018	0.018	>93
i	Regeneration test (C <sub>2</sub> H <sub>5</sub> OH)		1–3 h of reaction	63	9.8	73	13
j			15–48 h of reaction	18	2.1	21	10
k		<sup>13</sup> CO <sub>2</sub>	1–6 h of reaction	8.7	3.3	12	28
l			20–26 h of reaction	4.6	1.3	5.9	23

higher (74 %) because gas-phase <sup>13</sup>CO<sub>2</sub> was in equilibrium with the relatively stronger CO<sub>2</sub> adsorption site on TiO<sub>2</sub> [4–6] and the partial photodecomposition of Co-TCPP to form <sup>12</sup>CO<sub>2</sub> was also not negligible (Fig. S2). The activation step(s) was slower using moisture compared with that using H<sub>2</sub>. Similar to the time course using H<sub>2</sub>, the turning point of the CO formation rate was also observed at 9 h of reaction (Fig. S3A). Unfortunately, O<sub>2</sub> was not detected above the detection limit of GC-MS using Co-TCPP (2.5 wt %)-TiO<sub>2</sub> (Table 1a'''), indicating oxidative product could not be desorbed from TiO<sub>2</sub> (anatase phase) surface [16]. One of the plausible reactions was.



Co-TCPP (2.5 wt %)-TiO<sub>2</sub> was also prepared using JRC-TIO-6 (rutile phase) and tested for a photocatalytic test using <sup>13</sup>CO<sub>2</sub> (2.7 kPa) and H<sub>2</sub>O (1.7 kPa). In clear contrast to Fig. S3A, CO and O<sub>2</sub> were comparably formed (Fig. S3B) owing to the effective desorption of O<sub>2</sub> from rutile-phase TiO<sub>2</sub> [40,41]. On the other hand, the photocatalytic rates using Co-TCPP (2.5 wt %)-TiO<sub>2</sub> (rutile

phase) were lower than those using Co-TCPP (2.5 wt %)-TiO<sub>2</sub> (anatase phase) exclusively used in this paper (Fig. S3), leaving further catalyst design of Co-TCPP moiety anchored to preferable crystalline face of TiO<sub>2</sub> (anatase phase) in the proximity to preferable crystalline face of TiO<sub>2</sub> (rutile phase) in view of effective catalysis (Scheme 2A).

### 3.3. UV-visible spectra

Fig. 2 depicts UV-visible absorption spectra for H-TCPP compound and Co-TCPP complex in ethanol measured in transmission mode (panel A) and for each composite with TiO<sub>2</sub> measured in DR mode (panels B, C).

The major peaks centered at 415 and 427 nm in Fig. 2A originated from electronic transition from a<sub>1u</sub>(π) to e<sub>g</sub><sup>\*</sup>(π) states (Soret band) of H-TCPP and Co-TCPP, respectively (Scheme 2). The red peak shift for Co-TCPP compared to H-TCPP was consistent with the literature [42]. The a<sub>1u</sub>(π) state is with C<sub>4</sub> symmetry and populates on the N atoms of pyridine ring and connecting C atoms,

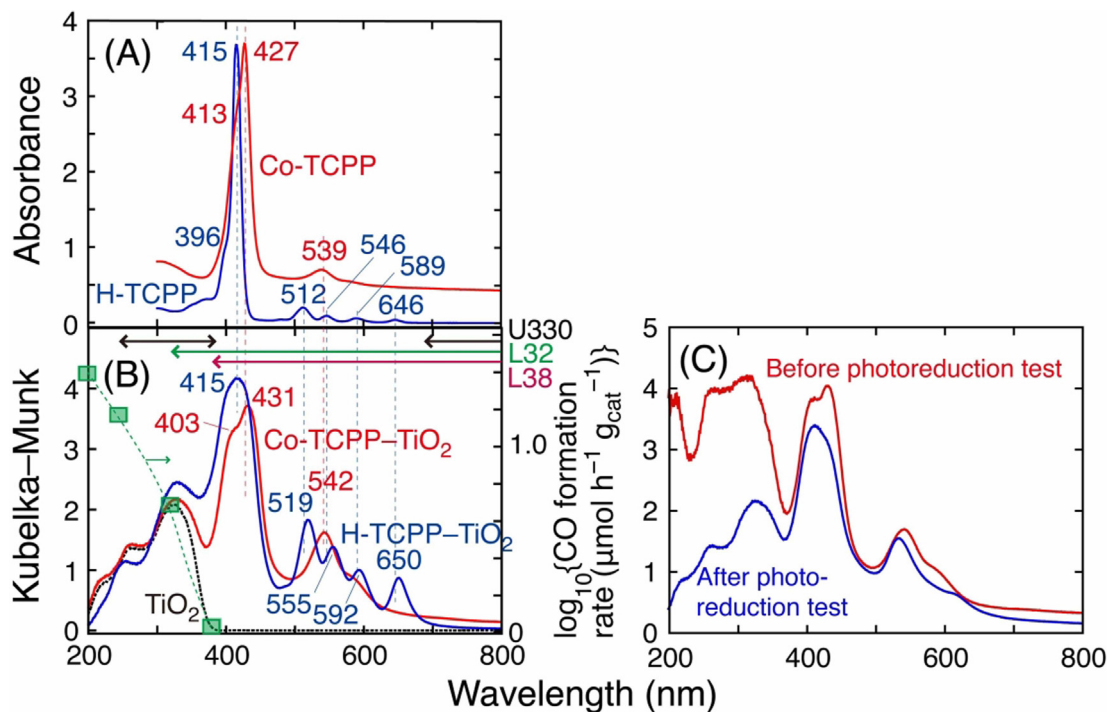


**Fig. 2.** UV-visible absorption spectra of (A) H-TCPP and Co-TCPP (1 mg each) dissolved in ethanol (5.6 mL; 0.23 and 0.21 mmol L<sup>-1</sup>, respectively). (B) TiO<sub>2</sub>, H-TCPP (2.5 wt %)-TiO<sub>2</sub>, and Co-TCPP (2.5 wt %)-TiO<sub>2</sub> composites and (C) Co-TCPP (2.5 wt %)-TiO<sub>2</sub> before and after photoreduction test under <sup>13</sup>CO<sub>2</sub>, H<sub>2</sub>, and UV-visible light irradiation. CO formation rates using filtered light (entries a–a'' in Table 1) in log scale are also drawn in panel B.

whereas the  $e_g^*(\pi)$  state is with C<sub>2</sub> symmetry and populates also on the N atoms and connecting C atoms on the basis of DFT calculations (Scheme 2B). The major peaks suggested stacking and aggregation of porphyrin units in which the Co center and N atom of the next Co-TCPP unit are connected in a head-to-tail fashion [36] (Scheme 1B) and/or H-aggregation (Scheme 1C) in which the Co centers are weakly bound and connected in a straight fashion [34,35,42] for H-TCPP and Co-TCPP.

The shoulder peak (396 and 413 nm, Fig. 2A) was attributed to each monomer, which is in agreement with the literature assigning the Soret peaks centered at 417, 427, and 430 nm to monomers, H-aggregates, and J-aggregates, respectively, for Zn-TTP [35] and the red shift to the aggregation of monomers for Co-TCPP [36].

The four weaker peaks that appeared at 512, 546, 589, and 646 nm were due to  $a_{2u}(\pi)$  to  $e_g^*(\pi)$  transitions (Q bands, Scheme 2) for H-TCPP, whereas the four peaks merged into two peaks at 539 nm (broad) and 585 nm (weak) for Co-TCPP, suggesting a higher symmetry for the porphyrin ring for Co-TCPP to preserve the degeneracy of the  $a_{2u}(\pi)$  orbital [43]. The  $a_{2u}(\pi)$  state is with C<sub>4</sub> symmetry and populates on the C atoms of pyridine ring, but not on the N atoms. The peak wavelength at 585 nm indicates a HOMO–LUMO gap of 2.12 eV.

Upon combination of porphyrins with TiO<sub>2</sub>, the absorption edge of TiO<sub>2</sub> appeared in the UV region between 380 and 330 nm (Fig. 2B), which is in accordance with the band gap for anatase-type TiO<sub>2</sub> (3.2 eV). Interestingly, the UV absorption edge was according to the plot of the CO formation rates in the CO<sub>2</sub> photoreduction tests (green squares in Fig. 2B, and entries a–a'' in Table 1), suggesting the critical role of charge separation of the TiO<sub>2</sub> band gap for the photoreduction of CO<sub>2</sub> into CO.

The Soret band for the H- and J-aggregates of H-TCPP on TiO<sub>2</sub> appeared at the same position as that in ethanol (415 nm), but it was significantly broadened by the interaction with the TiO<sub>2</sub> sur-

face (Fig. 2B). The H- and/or J-aggregates were still predominant, and a minor shoulder peak due to monomers was not well resolved because of the broadening. By contrast, the Soret band for the H- and/or J-aggregates of Co-TCPP shifted by + 4 nm, and that for monomers shifted by – 10 nm (Fig. 2A, B), strongly suggesting the interaction of Co-TCPP with the TiO<sub>2</sub> surface [44].

Upon interaction with the TiO<sub>2</sub> surface, the four Q band positions of H-TCPP red-shifted by 3–9 nm, and the major Q band for Co-TCPP shifted by 3 nm. The relative intensity compared with the Soret band significantly increased (Fig. 2B), suggesting a preferable interaction between the bridging C atoms connected to the carboxyphenyl group of H-TCPP and Co-TCPP [ $a_{1u}(\pi)$ , Scheme 2] and TiO<sub>2</sub> surface (edge interaction, Scheme 1D).

The fluorescence signal due to band gap emission was confirmed at 376 nm in the emission spectra (Fig. S4), and the major peak intensity progressively decreased as the Co-TCPP content in the composite was increased, suggesting the charge transfer from TiO<sub>2</sub> to Co-TCPP (Scheme 2A). One-electron and two-electron reductions to LUMO were also confirmed in the cyclic voltammetry (CV) of Co-TCPP (Fig. S5).

After the photocatalytic test using Co-TCPP (2.5 wt %)-TiO<sub>2</sub> under <sup>13</sup>CO<sub>2</sub>, H<sub>2</sub>, and UV-visible light irradiation for 48 h, the Soret band showed a clear change from a peak pattern due to the major J- and/or H-aggregates (a peak at 431 nm), accompanied with a smaller shoulder peak due to the Co-TCPP monomer (a shoulder peak at 403 nm) for the fresh photocatalyst, to a major peak at 412 nm due to the Co-TCPP monomer, accompanied with a weak shoulder peak due to the J- and/or H-aggregates at 435 nm (Fig. 2C).

The absorption in UV region apparently decreased after photocatalytic test under <sup>13</sup>CO<sub>2</sub>, H<sub>2</sub>, and UV-visible light (Fig. 2C) although it critically depended on the measurement conditions of UV-visible spectra (Fig. 2B). The decrease suggested reductive

decomposition of Co–TCPP during the test in addition to simple photodecomposition of Co–TCPP monitored in  $^{13}\text{CO}_2$  gas only (Fig. S2).

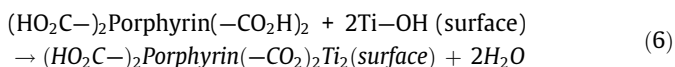
### 3.4. FTIR spectra

The binding mode of Co–TCPP on the  $\text{TiO}_2$  surface was investigated via FTIR. First, Co–TCPP crystals were thoroughly mixed with  $\text{TiO}_2$  at a ratio of 2.5 wt % Co–TCPP. Co–TCPP exhibited peaks at 1628 and 1408  $\text{cm}^{-1}$  (curve A in Fig. 3), which were characteristics of the  $\nu(\text{C}=\text{O})$  and  $\nu(\text{C}-\text{O})$  stretching vibrations of the carboxy group in TCPP, respectively (Scheme 1A) [45].

By contrast, upon supporting 2.5 wt % Co–TCPP on  $\text{TiO}_2$  from ethanol suspension (see Section 2, Experimental), the peak intensity at 1628  $\text{cm}^{-1}$  became weaker than that for the physical mixture, whereas a new peak centered at 1531  $\text{cm}^{-1}$  appeared (curve B in Fig. 3), which was ascribed to the asymmetric  $\nu_{\text{as}}(\text{CO}_2)$  stretching vibration of carboxylate (Scheme 1D). The peak at 1386  $\text{cm}^{-1}$  for Co–TCPP (2.5 wt %)- $\text{TiO}_2$  was assigned to the symmetric  $\nu_{\text{s}}(\text{CO}_2)$  stretching vibration of carboxylate overlapping with the  $\nu(\text{C}-\text{O})$  peak (1408  $\text{cm}^{-1}$ ), which is due to the remaining carboxy groups among the four carboxy groups for the original Co–TCPP (Scheme 1D).

The peaks at 1006 and 1176  $\text{cm}^{-1}$  were attributed to the  $\nu(\text{Co}-\text{N})$  and C–C skeleton vibration of the Co–TCPP benzene rings, respectively (curve A in Fig. 3) [46]. These peak positions did not change upon complexation with  $\text{TiO}_2$  (curve B in Fig. 3), but the intensities became 30 % of those for the physical mixture. In contrast to the isotropic orientation of the physical mixture of Co–TCPP molecules with  $\text{TiO}_2$  (curve A in Fig. 3), incident IR light transmits  $\text{TiO}_2$  disk and the Co–TCPP moiety would prefer to orient vertically (Scheme 1D). Thus, the vibration of the Co–N and C–C skeleton in the plane of the porphyrin ring is nearly perpendicular to the electric field vector of the incident IR light, and the peak intensity of these vibrations was relatively suppressed.

Based on UV–visible, fluorescence, and FTIR spectra (Figs. 2, 3, and S4), the neighboring two of the four carboxy groups of TCPP are dissociatively adsorbed on  $\text{TiO}_2$  [43,47]:



Here, a question arises why dehydrative immobilization of TCPP proceeded under  $\text{CO}_2$ ,  $\text{H}_2$ , and UV–visible light irradiation, in which water was a product associated with CO formation. A similar

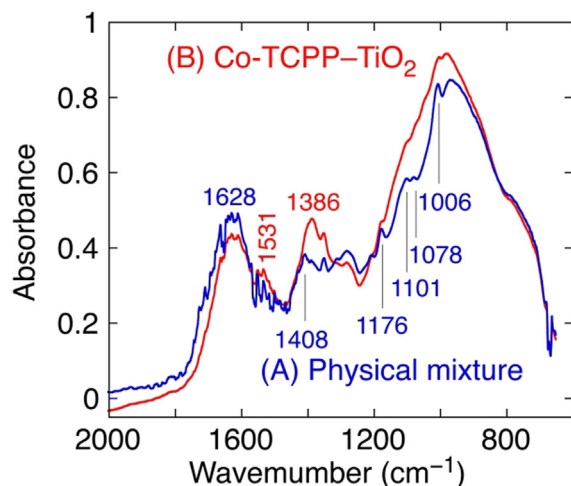


Fig. 3. FTIR spectra of (A) Co–TCPP (2.5 wt %) crystal physically mixed with  $\text{TiO}_2$  and (B) Co–TCPP (2.5 wt %)- $\text{TiO}_2$  composite.

immobilized structure of Co–tetraphenylporphyrins in Scheme 1D was reported on carbon surface via an organic synthetic route through diazocation on the phenyl group with C surface [19] as well as dehydration between carboxys of Co–TCPP with monolayer  $\text{TiO}_2$  on carbon [34]. By contrast, J- and/or H-aggregates were the major species on  $\text{TiO}_2$  for the fresh Co–TCPP- $\text{TiO}_2$  composites in this study. This comparison suggests the activation of hydroxy species with photogenerated hole ( $h^+$ ) to form hydroxy radical ( $\text{HO}\cdot$ ) on  $\text{TiO}_2$  [16]. In view of photocatalysis,  $\text{HO}\cdot$  radical should be related to  $\text{H}_2$  activation, leading to  $\text{CO}_2$  reduction on the Co sites by the following reaction mechanism (see the following Eqs. (10)–(16)).

Fig. 4 depicts the *in situ* FTIR spectra for  $\text{TiO}_2$  and Co–TCPP (2.5 wt %)- $\text{TiO}_2$  composite under  $^{13}\text{CO}_2$  (2.3 kPa),  $\text{H}_2$  (21.7 kPa), and UV–visible light irradiation at 295 K. The isotopic shift is calculated assuming harmonic oscillation on the basis of Eqs. (7) and (8):

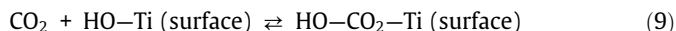
$$\nu = \frac{1}{2\pi c} \sqrt{\frac{k}{\mu}} \quad (7)$$

$$\frac{\nu_{^{13}\text{CO}}}{\nu_{^{12}\text{CO}}} = \sqrt{\frac{\frac{1}{13} + \frac{1}{16}}{\frac{1}{12} + \frac{1}{16}}} = 0.97778 \quad (8)$$

where  $\nu$  is the wave number,  $c$  is the speed of light,  $k$  is the force constant, and  $\mu$  is the reduced mass.

For  $\text{TiO}_2$  under  $^{13}\text{CO}_2$  (2.3 kPa) and  $\text{H}_2$  (21.7 kPa) for 30 min (red curve of subpanel i in Fig. 4A), an intense peak at 1471  $\text{cm}^{-1}$  and a shoulder peak at 1519  $\text{cm}^{-1}$  were assigned to  $\nu_{\text{as}}(\text{OCO})$  of carbonates (monodentate and/or bidentate), whereas another intense peak at 1330  $\text{cm}^{-1}$  and a shoulder peak at 1400  $\text{cm}^{-1}$  were assigned to their companion  $\nu_{\text{s}}(\text{OCO})$  peaks at 1635 and 1575  $\text{cm}^{-1}$  were assigned to  $\nu_{\text{as}}(\text{OCO})$  of bicarbonates (monodentate and/or bidentate), whereas the peaks at 1388 and 1220  $\text{cm}^{-1}$  were assigned to their companion  $\nu_{\text{s}}(\text{OCO})$  and  $\delta(\text{OH})$  bending vibration [48,49].

The broad negative peak at 3700  $\text{cm}^{-1}$  (red curve of subpanel ii in Fig. 4A) was a characteristic of  $\nu(\text{OH})$  of the hydroxy groups on the  $\text{TiO}_2$  surface [50], which were involved in the formation of bicarbonate combined with  $\text{CO}_2$ .



The FTIR spectrum for the Co–TCPP (2.5 wt %)- $\text{TiO}_2$  composite (red curve of subpanel i in Fig. 4B) was similar to that of  $\text{TiO}_2$ . The  $\text{CO}_2$  adsorption on Co–TCPP crystal was very limited (data not shown) because of their small heat of adsorption and smaller surface area compared with  $\text{TiO}_2$ .

Despite the UV–visible light irradiation, the peak intensities at 1519, 1471, and 1330  $\text{cm}^{-1}$  that are attributed to carbonates did not significantly change both for  $\text{TiO}_2$  (green curve of subpanel i in Fig. 4A) and Co–TCPP (2.5 wt %)- $\text{TiO}_2$  (green curve of subpanel i in Fig. 4B). By contrast, on the basis of the sharp  $\delta(\text{OH})$  peak at 1220  $\text{cm}^{-1}$ , bicarbonate species slowly decreased by 80 % in 15 h using  $\text{TiO}_2$ , whereas the peak quickly decreased by 80 % in 8 h using Co–TCPP (2.5 wt %)- $\text{TiO}_2$ . As the  $\nu(\text{OH})$  peak did not recover for both catalysts (subpanel ii in Fig. 4A, B) that were consumed via Eq. (9) (Scheme 1E, F), the bicarbonate did not decompose as the reverse reaction of Eq. (9) under UV–visible light irradiation. Nevertheless, it reacted with  $\text{H}_2$  to form  $^{13}\text{CO}_2$  and water for  $\text{TiO}_2$  and/or transformed to formate and water (Scheme 1F, G) for Co–TCPP (2.5 wt %)- $\text{TiO}_2$  as evidenced by the  $\nu_{\text{as}}(\text{OCO})$  peak at 1560  $\text{cm}^{-1}$  owing to formate [6] (subpanel i in Fig. 4B).

The absorbance in the area around 1628, 1531, and 1386  $\text{cm}^{-1}$  owing to terminal ligands of TCPP (Fig. 3) in general decreased for Co–TCPP- $\text{TiO}_2$  sample under UV–visible light irradiation (Fig. 4B-i)

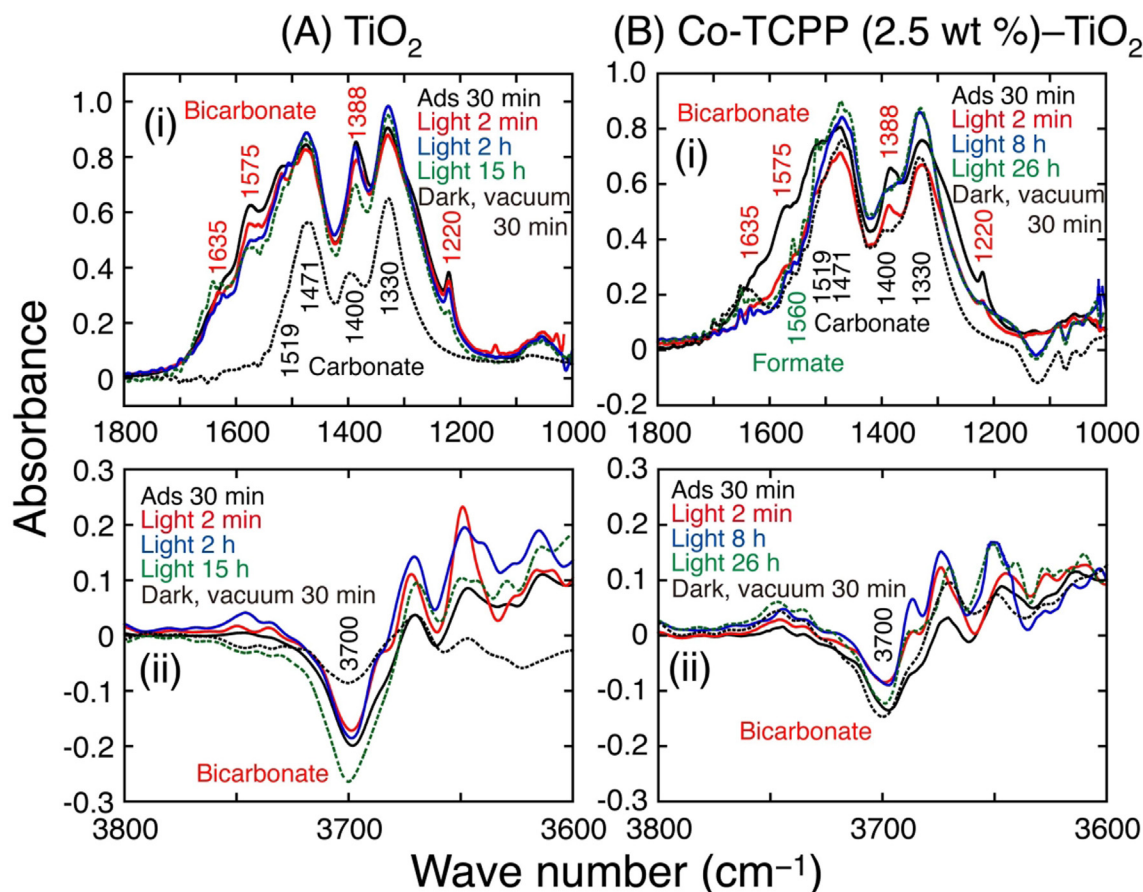
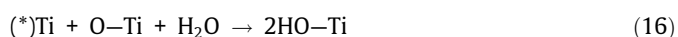
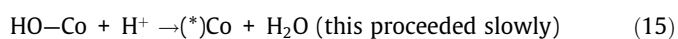
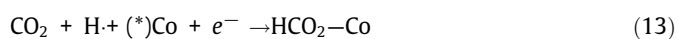
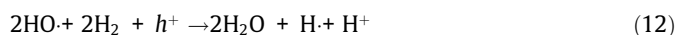


Fig. 4. FTIR spectra of (A)  $\text{TiO}_2$  and (B) Co-TCPP (2.5 wt %)- $\text{TiO}_2$  under  $^{13}\text{CO}_2$  (2.3 kPa),  $\text{H}_2$  (21.7 kPa), and UV-visible light irradiation.

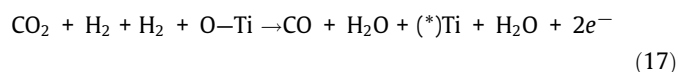
to more extent in comparison to the monitoring for  $\text{TiO}_2$  sample under similar conditions (Fig. 4A-i). This contrast suggested simple (Fig. S2) and/or reductive decomposition of Co-TCPP (Fig. 2C).

The negative peak of isolated hydroxy species ( $3700\text{ cm}^{-1}$ ) and positive peaks of not isolated hydroxy species ( $3674\text{--}3671$  and  $3650\text{ cm}^{-1}$ ) were commonly observed both on  $\text{TiO}_2$  and Co-TCPP- $\text{TiO}_2$  (Fig. 4A-ii, B-ii) [51]. In contrast, the hydroxy peak at  $3686\text{ cm}^{-1}$  was detected only for Co-TCPP- $\text{TiO}_2$  (Fig. 4B-ii) [51], suggesting reactive hydroxy species for Co-TCPP- $\text{TiO}_2$ , e.g. at the interface between  $\text{TiO}_2$  and Co-TCPP (Scheme 2A).

We recall the hydroxy activation of  $\text{TiO}_2$  by UV light as suggested in the discussion on the binding mode analysis of Co-TCPP (Fig. 3) for  $\text{H}_2$  activation:



where the asterisk denotes surface vacant site. The formates in Eqs. (13) and (14) could be formed also via bicarbonates (Fig. 4B). The different reactivity of bicarbonate on  $\text{TiO}_2$  and Co-TCPP (2.5 wt %)- $\text{TiO}_2$  was because Co-TCPP-anchored formate was formed from bicarbonate on  $\text{TiO}_2$  (Scheme 1F, G). The overall reaction is obtained by summing Eqs. (10)–(16).



Thus, the photoreduction of  $\text{CO}_2$  into CO proceeded while the reduction of surface O of  $\text{TiO}_2$  should be irreversible.

Then, the light was turned off and the samples were evacuated for 30 min. On  $\text{TiO}_2$ , the bicarbonates were totally removed, and the  $\nu(\text{OH})$  peak recovered to the original level (subpanel ii in Fig. 4A), suggesting exclusive decomposition of bicarbonate back to  $^{13}\text{CO}_2$  and hydroxy group. By clear contrast, the  $\nu(\text{OH})$  negative peak at  $3700\text{ cm}^{-1}$  essentially remained the same under vacuum for 30 min using Co-TCPP (2.5 wt %)- $\text{TiO}_2$  (subpanel ii in Fig. 4B), suggesting Co-anchored formate species were stable under vacuum (Scheme 1G and Eq. (13)). Similarly, the physisorption of CO on Cu or Fe atoms through van der Waals forces results in the formation of a strongly bound formate by overcoming an activation energy barrier [52]. The carbonate peaks decreased by 30 % for  $\text{TiO}_2$  under vacuum for 30 min, suggesting the reverse reaction of Eq. (18), whereas the decrease was only 5 % for Co-TCPP (2.5 wt %)- $\text{TiO}_2$  probably because of the effects of Co-TCPP species.



Finally, as shown in Fig. 4B (subpanel i), two negative peaks appeared at 1121 and 1070  $\text{cm}^{-1}$  under continuous light irradiation, which were not found in either  $\text{TiO}_2$  moiety or Co-TCPP crystal probably because of the irreversible deformation of the Co-TCPP- $\text{TiO}_2$  composite.

In summary, for the Co-TCPP (2.5 wt %)- $\text{TiO}_2$  composite,  $\text{CO}_2$  was mainly adsorbed on  $\text{TiO}_2$ , and a different reactivity on the formation of formate via bicarbonates was suggested by the ligation to Co. In the absence of the stabilization effect of Co, bicarbonates were easily decomposed into  $^{13}\text{CO}_2$  and water by  $\text{H}_2$ .

### 3.5. HR-TEM

HR-TEM images were observed for Co-TCPP crystal. The lattice fringes with the intervals of 0.348 nm (image A1 in Fig. 5) and 1.34 nm (image A2 in Fig. 5) were observed, demonstrating the Co-TCPP stacking interval and the interval between stacked Co-TCPP, respectively [53].

In the images for Co-TCPP (2.5 wt %)- $\text{TiO}_2$  composite, lattice fringes with the intervals of 0.210, 0.232, 0.239, 0.241–0.250, and 0.336–0.350 nm were observed because of the diffractions by the

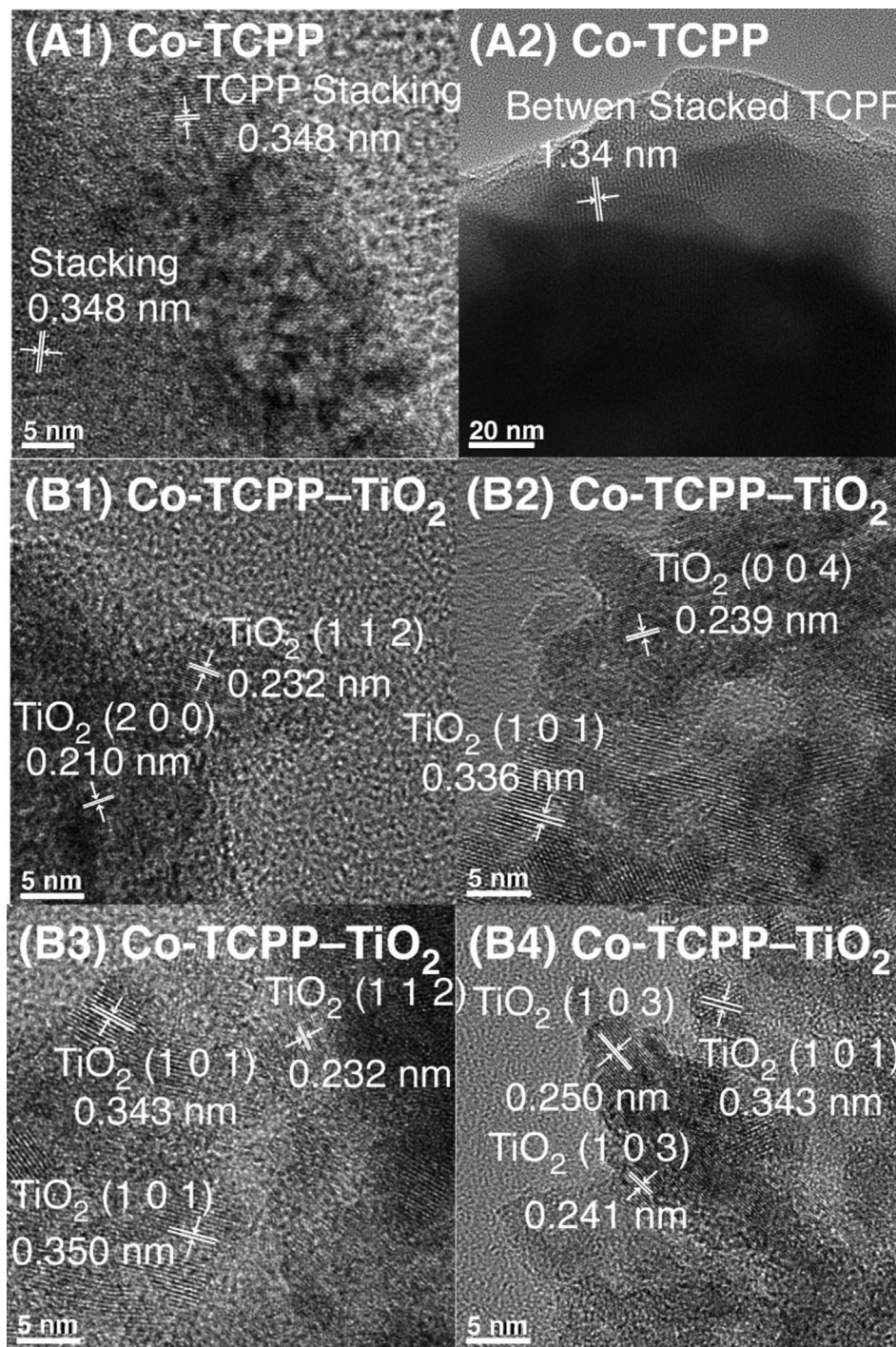


Fig. 5. HR-TEM images of (A1, A2) Co-TCPP and (B1–B4) Co-TCPP (2.5 wt %)- $\text{TiO}_2$ .

(200), (112), (004), (103), and (101) faces (theoretical values of 0.1893, 0.2333, 0.2379, 0.2431, and 0.3517 nm, respectively) (see [Supplementary materials](#) for assignment) of anatase-phase TiO<sub>2</sub> (images B1–B4 in [Fig. 5](#)). Predominant lattices observed in the HR-TEM images were in consistent with exclusive X-ray diffraction peaks of anatase-phase TiO<sub>2</sub> ([Fig. S6](#)).

### 3.6. XAFS spectra

The coordination of the central Co atom in TCPP during CO<sub>2</sub> photoreduction was monitored by X-ray absorption near-edge structure (XANES) and EXAFS under photocatalytic conditions. Co-TCPP (25 wt %)-TiO<sub>2</sub> was used because the X-ray absorbance of the most active Co-TCPP (2.5 wt %)-TiO<sub>2</sub> was insufficient for quantitative EXAFS data analysis measured in transmission mode. Nevertheless, the angular photoelectron wave number  $k^3$  multiplied by normalized EXAFS  $\chi$  function was qualitatively common between the two samples ([Fig. S7](#)), and the coordination information obtained from EXAFS analyses can be adapted also for the most active Co-TCPP (2.5 wt %)-TiO<sub>2</sub> photocatalyst.

The pre-edge peaks at 7710 and 7716 eV were attributed to 1 s–3d and 1 s–4p transitions irrelevant to the presence or absence of reactants (panel A in [Fig. 6](#)), reflecting the square planar coordination of the Co–N<sub>4</sub> center with D<sub>4h</sub> symmetry ([Schemes 1A and 2](#)) [12]. Based on relatively similar absorption edge energy position

for CoO and Co-TCPP–TiO<sub>2</sub>, the valence state of Co in Co-TCPP should be close or equal to 2+, which is consistent with the CV study for Co-TCPP ([Fig. S5](#)).

[Fig. 6](#) (panel B) depicts the time-course change of whiteline peak intensity of Co-TCPP (25 wt %)-TiO<sub>2</sub> under CO<sub>2</sub>, H<sub>2</sub>, and UV–visible light irradiation. When the light was turned on, the intensity quickly became weaker by 4.1 % under Ar and by 6.4 % under CO<sub>2</sub> and H<sub>2</sub>, indicating the electron excitation to CB of TiO<sub>2</sub> because of UV light energy, followed by the transfer to the Co sites ([Scheme 2A](#)). In the time course, the intensity was lower by 2.4 %–6.1 % in the presence of CO<sub>2</sub> and H<sub>2</sub> compared with that under Ar, suggesting that the ligand-to-metal charge transfer from coordinated CO<sub>2</sub>  $\pi$  orbital(s) to empty 3d orbital(s) of Co further reduced Co.

After the UV–visible light was turned on, the white line peak intensity soon reached an equilibrium either under Ar or under CO<sub>2</sub> and H<sub>2</sub> (panel B in [Fig. 6](#)), inferring an equilibrium of electron transfer from TiO<sub>2</sub> to Co and charge recombination. Nevertheless, a gradual increase of the intensity by 2.3 % during 70 and 150 min of reaction was observed because the major species on the Co site transformed from formate into hydroxy ([Scheme 1G, H](#)) using the Co-TCPP (25 wt %)-TiO<sub>2</sub> photocatalyst because the hydroxy group withdraws electrons more effectively than formate.

The major J- and/or H-aggregates of Co-TCPP molecules were gradually separated by the reaction of surface hydroxy of TiO<sub>2</sub>

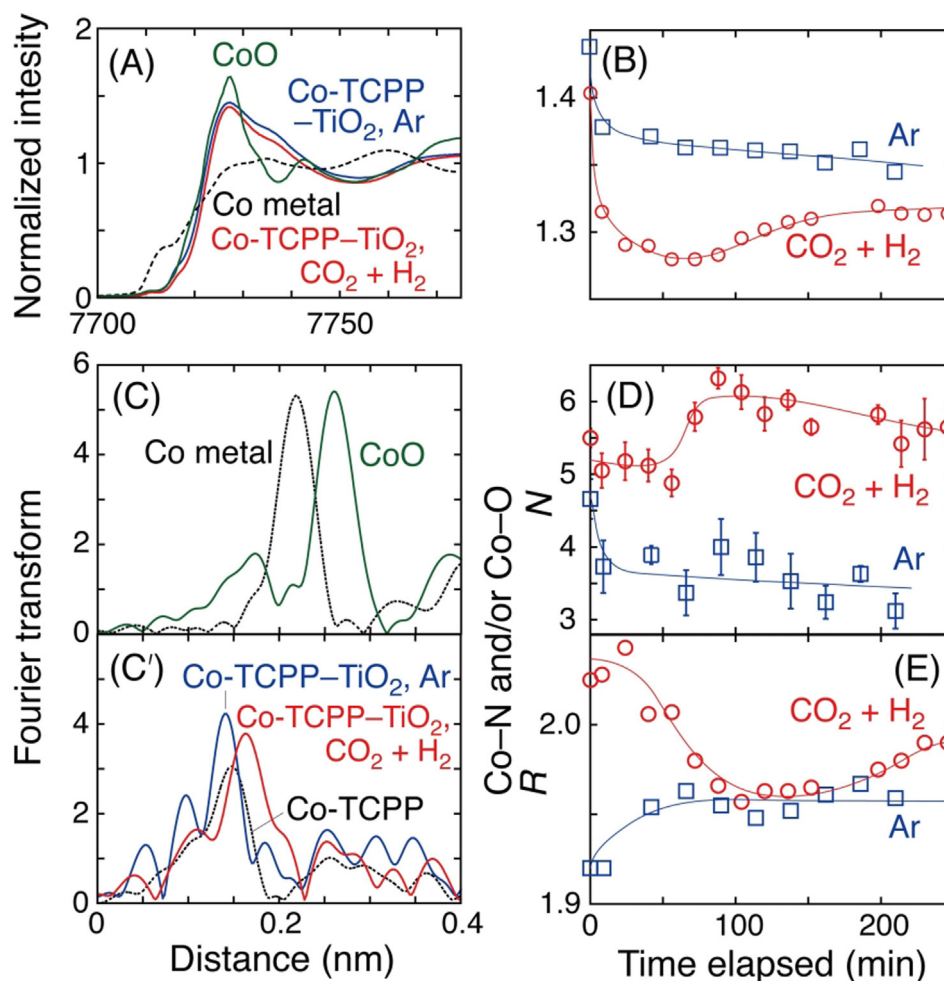


**Fig. 6.** (A) Normalized XANES spectra of Co metal, CoO, and Co-TCPP (25 wt %)-TiO<sub>2</sub> under Ar and under CO<sub>2</sub> (2.7 kPa) and H<sub>2</sub> (20.7 kPa). (B) Time course of normalized white line intensities of Co-TCPP (25 wt %)-TiO<sub>2</sub> under Ar (blue) and under CO<sub>2</sub> and H<sub>2</sub> (red). (C, C') Fourier transform of EXAFS spectra at Co K-edge of the Co metal foil, CoO, Co-TCPP (25 wt %)-TiO<sub>2</sub> under Ar, and Co-TCPP (25 wt %)-TiO<sub>2</sub> under CO<sub>2</sub> and H<sub>2</sub>. Time course of (D) coordination number and (E) interatomic distance of Co–N under Ar and Co–O and/or Co–N under CO<sub>2</sub> and H<sub>2</sub> for the Co-TCPP (25 wt %)-TiO<sub>2</sub> photocatalyst.

prompted by light activation (Eq. (6)). Hence, formate generation was accelerated via Eq. (13) and/or via reductive transfer of bicarbonate on TiO<sub>2</sub> (subpanel i in Fig. 4B and Scheme 1F), which was related to the decrease of the *N* value of Co–N of Co–TCPP units over TiO<sub>2</sub>: from 4.7 before light irradiation to 3.4 under Ar and UV–visible light irradiation (blue squares of panel D in Fig. 6). However, the decrease may be also related to the partial photodecomposition of Co–TCPP at carboxy sites (2.9 CO<sub>2</sub> per Co–TCPP in 10 h of UV–visible light irradiation, Fig. S2 and Scheme 1).

In the Fourier transform of *k*<sup>3</sup>-weighted EXAFS  $\chi$  oscillation (panels C and C' in Fig. 6), the peak at 0.142 nm (phase shift uncorrected) for Co–TCPP (2.5 wt %)-TiO<sub>2</sub> under Ar was attributed to Co–N interatomic pair [13,51], which is almost at the same distance as that for the peak of Co–TCPP crystals (panel C' in Fig. 6). The best-fit result was *N* value of 4.7 (with an error of  $\pm 0.2$ ), which is associated with an interatomic distance (*R*) value of 0.192 nm (panels D and E in Fig. 6). As the stacking of Co–TCPP units was observed with an interval of 0.348 nm (subpanel A1 in Fig. 5), the interunit coordination between Co and N was by far longer than the Co–N coordination in porphyrin. Hence, the variation of the *N* value was mostly due to the axial coordination to Co due to the increased population of monomer unit over TiO<sub>2</sub> (Scheme 1F). A significant portion of the Co–TCPP units became the monomer on TiO<sub>2</sub> under the photocatalytic reaction conditions, and the coordination to Co by water and/or CO<sub>2</sub> from air should increase the *N* value.

Under CO<sub>2</sub> and H<sub>2</sub>, the peak at 0.142 nm under Ar shifted to 0.163 nm (phase shift uncorrected, panel C' in Fig. 6). The best-fit result was an *R* value of 0.203 nm associated with *N* of 5.5 (with an error of  $\pm 0.1$ , panels D and E in Fig. 6). This increase suggested CO<sub>2</sub> coordination to Co in a significant portion of the monomeric Co–TCPP unit because no formate peak appeared under CO<sub>2</sub> and H<sub>2</sub> in the absence of UV–visible light irradiation (subpanel i in Fig. 4B).

When Co–TCPP–TiO<sub>2</sub> under Ar was irradiated by UV–visible light, the *N* value for Co–N interatomic pair gradually decreased from 4.6 to 3.6 in 70 min and the *R* value for Co–N interatomic pair was 0.193–0.195 nm in 40 min (panels D and E in Fig. 6), suggesting coordinated water/CO<sub>2</sub> desorption under light irradiation from monomeric Co site and/or partial photodecomposition of Co–TCPP at carboxy sites (Scheme 1) affected the coordination of central Co site.

Under CO<sub>2</sub>, H<sub>2</sub>, and UV–visible light irradiation, the *N* value for Co–N increased from 5.5 to 5.8–6.3 in 70–140 min (panels D and E in Fig. 6), suggesting formate and/or hydroxy formation on Co (Scheme 1G, H) via Eqs. (13) and (14) and/or reductive transfer of bicarbonate on TiO<sub>2</sub> as suggested by FTIR (subpanel i in Fig. 4B), and the first shell was actually both Co–N and Co–O interatomic pairs. Accordingly, the *R* value for Co–N and Co–O interatomic pairs gradually decreased from 0.203 to 0.196 nm after 80 min of light irradiation (panel E in Fig. 6).

In the UV–visible absorption spectra of the sample used for 48 h of photoreduction test under <sup>13</sup>CO<sub>2</sub>, H<sub>2</sub>, and UV–visible light irradiation (Fig. 2C), the peak at 431 nm that is attributed to the J- and/or H-aggregates became weaker, and the peak at 403 nm that is attributed to the monomeric Co–TCPP unit became major, supporting covalent anchoring of the Co–TCPP unit on TiO<sub>2</sub> via Eq. (6) by the effects of very reactive HO· radical under the irradiation of UV–visible light in consistent with EXAFS results.

Unexpectedly, when the used Co–TCPP–TiO<sub>2</sub> photocatalyst under the UV–visible light irradiation ( $\lambda > 320$  nm) was exposed to air for 5 days, the UV–visible absorption spectrum became similar to that of the fresh sample (Fig. S8A), and the CO formation rate under <sup>13</sup>CO<sub>2</sub>, H<sub>2</sub>, and UV–visible light irradiation ( $\lambda > 320$  nm) in the second test was 1.62  $\mu\text{mol h}^{-1} \text{g}_{\text{cat}}^{-1}$  (Fig. S8B), which was higher by 1.54 times than the rate after 9 h of reaction in the first test (Fig. S8B). The monomeric Co–TCPP would hydrate in ambient con-

ditions and form J- and/or H-aggregates. However, major reasons were not only the decomposition of monomeric Co–TCPP hydroxy species but also the oxidation of the reduced Ti(\*) site in Eq. (17) also affected the reactivation of the Co–TCPP–TiO<sub>2</sub> photocatalyst.

### 3.7. Reactivation of Co–TCPP (2.5 wt %)-TiO<sub>2</sub> catalyst

Finally, we attempted to reactivate the Co–TCPP (2.5 wt %)-TiO<sub>2</sub> photocatalyst that was used in a test under <sup>13</sup>CO<sub>2</sub>, H<sub>2</sub>, and UV–visible light irradiation for 48 h on the basis of partial reactivation under ambient air (Fig. S8) and also on the mechanistic knowledge previously discussed. The color of Co–TCPP (2.5 wt %)-TiO<sub>2</sub> slightly changed from dark orange similar to that of its fresh state to dark saffron after 48 h of the photoreaction test. When the catalyst was treated with H<sub>2</sub> and UV–visible light, the <sup>13</sup>CO formation rate was very similar to relatively deactivated one after 9 h of a photoreaction in the first test (panel C of Fig. 1, entries b, e, and f in Table 2). With H<sub>2</sub> treatment, <sup>12</sup>CO formation became negligible because H<sub>2</sub> treatment under UV–visible light irradiation removed CO<sub>2</sub> on the relatively stronger adsorption site.

When the catalyst was treated with O<sub>2</sub> and UV–visible light, the color of the catalyst changed from dark saffron to light gray, and CO formation was below the detection limit of GC–MS or negligible (entries g and h in Table 2). Contrary to the expected results, the O<sub>2</sub> treatment completely decomposed the Co–TCPP units.

By contrast, when the catalyst was treated with ethanol (2.7 kPa) and UV–visible light, the <sup>13</sup>CO formation rate increased by 3.6 times compared with the initial rate in the first test (panels C and D of Fig. 1; entries a and i in Table 2). The turnover of CO<sub>2</sub> into CO until 3 h of reaction in the second test was 7.4. Interestingly, in the second test, the <sup>13</sup>CO formation rate did not change during 8 h of reaction. In the regeneration test, after 8 h of reaction, the <sup>13</sup>CO formation rate became 18  $\mu\text{mol h}^{-1} \text{g}_{\text{cat}}^{-1}$ , which was comparable with the initial rate in the first test (17  $\mu\text{mol h}^{-1} \text{g}_{\text{cat}}^{-1}$ ; entries a and j in Table 2). The CO formation rate increased to 73–21  $\mu\text{mol h}^{-1} \text{g}_{\text{cat}}^{-1}$ , and the <sup>12</sup>CO ratio decreased to 13–10 mol % (entries i and j in Table 2) because the reaction step(s) later than the equilibrium between <sup>13</sup>CO<sub>2</sub> gas and relatively strong adsorption site of CO<sub>2</sub> on TiO<sub>2</sub> proceeded faster because of the contribution of the monomeric Co–TCPP units on TiO<sub>2</sub>. As the partial photodecomposition of Co–TCPP essentially completed until 10 h of the first photoreaction test (Fig. S2), the contribution of <sup>12</sup>CO<sub>2</sub> derived from the decomposition is low for the <sup>12</sup>CO formation.

The reason of reactivation of Co–TCPP (2.5 wt %)-TiO<sub>2</sub> was investigated using Co K-edge EXAFS (Fig. 7A). The coordination at single Co site basically retained during the reactivation tests using ethanol and UV–visible light. In a closer look, Co–N coordination number (4) for fresh catalyst decreased to 3.5 after the photocatalytic test (a peak at 0.14 nm, phase shift uncorrected, Fig. 7B-b) mostly due to the deformation and/or partial/reductive decomposition of Co–TCPP (Fig. S2 and Scheme 1G, H). The coordination number further decreased to 3.1 after the reactivation using ethanol and UV–visible light (a peak at 0.14 nm, phase shift uncorrected, Fig. 7B-c) due to the formation of unsaturated Co site by the removal of hydroxy group using ethanol (Scheme 1G, H) enabling the highest <sup>13</sup>CO formation rate: 63  $\mu\text{mol h}^{-1} \text{g}_{\text{cat}}^{-1}$ .

The Co K-edge XANES spectra were also compared for fresh Co–TCPP (2.5 wt %)-TiO<sub>2</sub> (Fig. 6A and 7C-a), the catalyst under CO<sub>2</sub> and H<sub>2</sub> before (Fig. 6A), and after 17-h irradiation of UV–visible light (Fig. 7C-b), and the catalyst of Fig. 7C-b reactivated under ethanol and UV–visible light for 5 min (Fig. 7C-c). These XANES pattern basically retained very similar pattern, demonstrating the retention of single Co site coordinated by TCPP ligand (Scheme 1). In a closer look, the intensity of pre-edge peak at 7712 eV progressively decreased by CO<sub>2</sub> photoreduction test (Fig. 7C-b) then reactivation under ethanol and UV–visible light (Fig. 7C-c), suggesting gradual

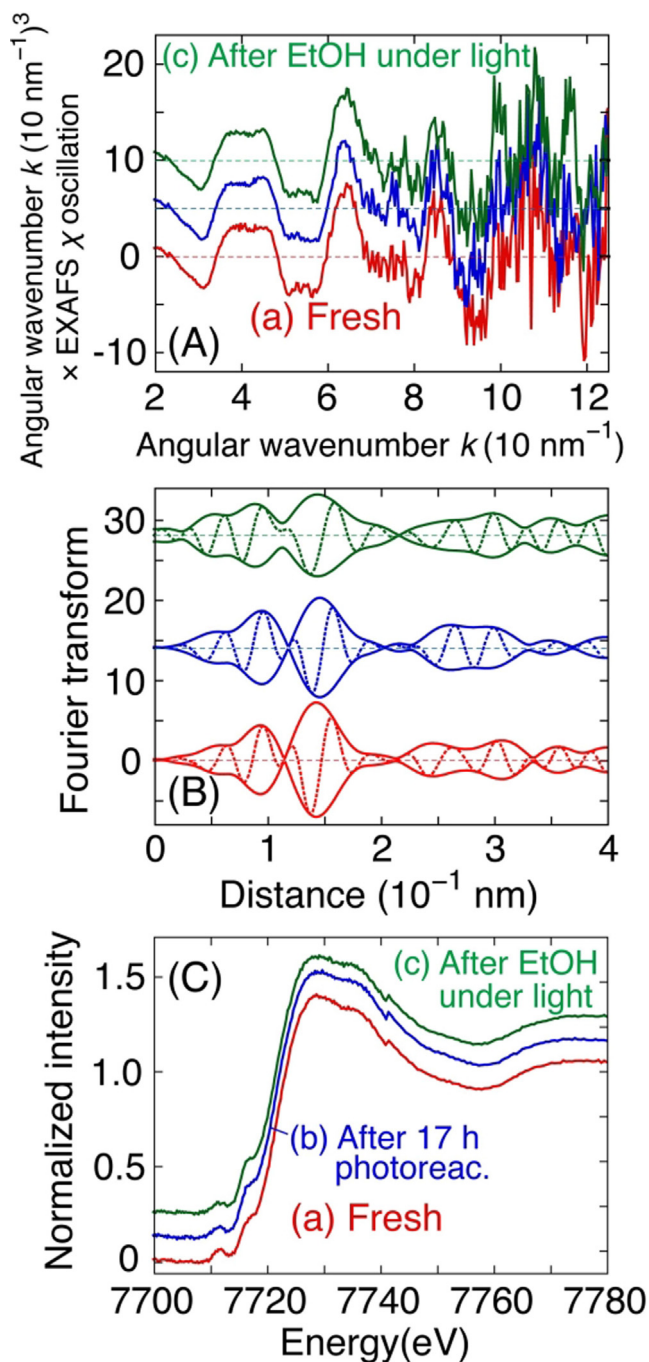


**Fig. 7.** (A)  $k^3\chi$  and (B) its associated Fourier transform of Co K-edge EXAFS of Co-TCPP (2.5 wt %)-TiO<sub>2</sub> as fresh, 1 h evacuated (a), after photoreduction test using CO<sub>2</sub> (2.7 kPa) H<sub>2</sub> (20.7 kPa) and UV-visible light for 17 h (b), and after subsequent treatment using C<sub>2</sub>H<sub>5</sub>OH (2.7 kPa) and UV-visible light for 5 min (c).

reduction of single Co ion site. The reductive decomposition of TCPP was still minor under CO<sub>2</sub>, H<sub>2</sub>, and light for 17 h and/or under ethanol and light for 5 min. When the reductive decomposition became even serious under ethanol and light, serious deactivation of the Co-TCPP-TiO<sub>2</sub> photocatalyst was observed (see below).

We further tried repeated reactivation using ethanol (2.7 kPa) and UV-visible light irradiation (Fig. S9). After the second reactivation, the highest <sup>13</sup>CO formation rate ( $67 \mu\text{mol h}^{-1} \text{g}_{\text{cat}}^{-1}$ ) was not achieved but essentially the same rate as the test for fresh catalyst was obtained ( $18 \mu\text{mol h}^{-1} \text{g}_{\text{cat}}^{-1}$ ). The rate later than 8 h of reaction was  $5.5 \mu\text{mol h}^{-1} \text{g}_{\text{cat}}^{-1}$  that was higher by 1.8–2.4 times compared

to the dropped rates for fresh catalyst (panels A and C of Fig. S9 and Table 2b) due to the removal of hydroxy attached to Co and partial deformation of central Co site. By the careful reactivation, supported porphyrin photocatalysts would be utilized sustainably.

Control tests were also performed to verify the hydrogen source for CO<sub>2</sub> reduction reaction. After the first 48-h test and reactivation using ethanol of UV-visible light for 5 min, a test was done under <sup>13</sup>CO<sub>2</sub> and UV-visible light. The initial <sup>13</sup>CO formation rate was lower by 50 % compared to corresponding rate of fresh catalyst (Fig. 1C and E and Table 2a and k) and 14 % of corresponding rate of reactivation test under <sup>13</sup>CO<sub>2</sub>, H<sub>2</sub>, and UV-visible light (Fig. 1D and E and Table 2i and k). Thus, the contribution of adsorbed ethanol and/or ethanol-derived species to photocatalytic CO formation as hydrogen source was minor.

Based on similar point of view, a control test was also performed using fresh Co-TCPP (2.5 wt %)-TiO<sub>2</sub> catalyst under <sup>13</sup>CO<sub>2</sub>, C<sub>2</sub>H<sub>5</sub>OH, and UV-visible light (Fig. 1F). The initial <sup>13</sup>CO formation rate ( $16 \mu\text{mol h}^{-1} \text{g}_{\text{cat}}^{-1}$ ) was essential equivalent to one of test under <sup>13</sup>CO<sub>2</sub>, H<sub>2</sub>, and UV-visible light ( $17 \mu\text{mol h}^{-1} \text{g}_{\text{cat}}^{-1}$ ; Table 2a and c). Furthermore, the <sup>13</sup>CO formation quickly deactivated at 3 h of reaction, and the rate after 3 h of reaction was very low ( $1.5 \mu\text{mol h}^{-1} \text{g}_{\text{cat}}^{-1}$ ; Table 2d). Thus, ethanol was found to be a double-edged sword for Co-TCPP (2.5 wt %)-TiO<sub>2</sub> photocatalyst. While ethanol was equivalent reducing agent to H<sub>2</sub> in view of initial <sup>13</sup>CO formation, it also quickly decomposed TCPP ligand as evident from the quick <sup>12</sup>CO formation derived from TCPP at rates of 26–15  $\mu\text{mol h}^{-1} \text{g}_{\text{cat}}^{-1}$  (Table 2c and d).

Ethanol effectively removed the ligand blocking the central Co site and supplied sufficient electrons to the Co-TCPP moiety. However, TCPP framework slowly decomposed under relatively harsh reductive conditions. To avoid this problem, to enforce the porphyrin ligand by even greater conjugate system should improve the stability of the catalyst in this study [54–56].

Recently, several selective photocatalysts, e.g. Ni-ZrO<sub>2</sub> and Co-ZrO<sub>2</sub>, to convert CO into value-added hydrocarbons were reported [6,57]. Co-TCPP/TiO<sub>2</sub> that was selective to CO formation in this study will be more valuable when metal nanoparticles (Ni or Co) were mixed or accommodated in the catalyst.

#### 4. Conclusions

Using Co-TCPP (2.5 wt %)-TiO<sub>2</sub> under <sup>13</sup>CO<sub>2</sub>, H<sub>2</sub>, and UV-visible light irradiation, CO was generated at a maximum rate of  $2.5 \mu\text{mol h}^{-1}$  (using 100 mg of catalyst and UV-visible light of  $118 \text{ mW cm}^{-2}$ ). The photocatalyst amount and light intensity were common in this study. The transformation of the J- and/or H-aggregates of Co-TCPP to isolated monomers anchored on TiO<sub>2</sub> proceeded via dehydration between the carboxy group and the hydroxy group of TiO<sub>2</sub> by the effects of hydroxy radicals on TiO<sub>2</sub>, which were activated under UV light. The uncoordinated Co site was essential for the stabilization of formate that will be further reduced to CO as the product. Moreover, the remaining hydroxy and/or O after the CO evolution on Co and simple and/or reductive partial decomposition of Co-TCPP caused the serious deactivation of the catalyst. Unexpectedly, partial reactivation of the used photocatalysts was possible by leaving the used catalyst in the air for 5 days because the partially irreversibly reduced TiO<sub>2</sub> surface was again oxidized by reaction with O<sub>2</sub> in the air. However, reactivation of the reduced TiO<sub>2</sub> surface was still partial. Ethanol treatment of the used Co-TCPP (2.5 wt %)-TiO<sub>2</sub> photocatalyst under UV-visible light irradiation was conducted for further reactivation, resulting in 3.6 and 3.0 times higher <sup>13</sup>CO and total CO formation rates compared with values using the fresh photocatalyst, and the turnover was 7.4 during 3 h of photocatalytic reaction. Reactivation under ethanol and UV-visible light must be within short period because

ethanol removed not only coordinated hydroxy on Co site but proceeded significant reductive decomposition of TCPP demonstrated as an evolution of  $^{12}\text{C}$ O when ethanol was utilized as a reductant instead of  $\text{H}_2$ . This study paves the way to provide a general method to reactivate single-site metal complex photocatalysts anchored on semiconductors.

### Declaration of Competing Interest

The authors declare that they have no known competing financial interests or personal relationships that could have appeared to influence the work reported in this paper.

### Acknowledgments

The authors are grateful for the financial support from the Grant-in-Aid for Scientific Research B (20H02834) and C (17 K05961) from the Japan Society for the Promotion of Science. X-ray absorption experiments were performed with the approval of the Photon Factory Proposal Review Committee (2020G676 and 2018G649).

### Appendix A. Supplementary material

The following files are available free of charge:

The Experimental methods section provides details on photocatalytic  $^{13}\text{C}$ O<sub>2</sub> reduction, the absorption–fluorescence spectra, CV, and XRD measurements. (file type, MS Word).

Results and discussion covers the dependences of CO formation rate on the amount of photocatalysts and also on the Co–TCPP content in photocatalysts, time-course profile of the  $^{13}\text{C}$ O<sub>2</sub> exchange test, time-course profiles of the photocatalytic tests under  $^{13}\text{C}$ O<sub>2</sub> and  $\text{H}_2\text{O}$ , fluorescence spectra of photocatalysts, CV of Co–TCPP, XRD of the photocatalysts, information for HR-TEM, EXAFS comparison depending on the Co–TCPP content in the photocatalysts, and results on the reuse of the photocatalysts after reactivation. (file type, MS Word).

Supplementary data to this article can be found online at <https://doi.org/10.1016/j.jcat.2022.07.006>.

### References

- Y. Izumi, Recent Advances in the Photocatalytic Conversion of Carbon Dioxide to Fuels with Water and/or Hydrogen Using Solar Energy and Beyond, *Coord. Chem. Rev.* 257 (2013) 171–186.
- A. Goeppert, M. Czaun, J.-P. Jones, G.K. Surya Prakash, G.A. Olah, Recycling of Carbon Dioxide to Methanol and Derived Products – Closing the Loop, *Chem. Soc. Rev.* 43 (23) (2014) 7995–8048.
- J. Albero, Y. Peng, H. García, Photocatalytic CO<sub>2</sub> Reduction to C<sub>2</sub>-Products, *ACS Catal.* 10 (2020) 5734–5749.
- H. Zhang, T. Itoi, T. Konishi, Y. Izumi, Dual Photocatalytic Roles of Light: Charge Separation at the Band Gap and Heat via Localized Surface Plasmon Resonance to Convert CO<sub>2</sub> into CO over Silver-Zirconium Oxide, *J. Am. Chem. Soc.* 141 (2019) 6292–6301.
- H. Zhang, T. Itoi, K. Niki, T. Konishi, Y. Izumi, Dual Origins of Photocatalysis: Light-induced Band-gap Excitation of Zirconium Oxide and Ambient Heat Activation of Gold to Enable  $^{13}\text{C}$ O<sub>2</sub> Photoreduction/Conversion, *Catal. Today* 356 (2020) 544–556.
- H. Zhang, T. Itoi, T. Konishi, Y. Izumi, Efficient and Selective Interplay Revealed: CO<sub>2</sub> Reduction to CO over ZrO<sub>2</sub> by Light with Further Reduction to Methane over Ni<sup>0</sup> by Heat Converted from Light, *Angew. Chem. Int. Ed.* 60 (2021) 9045–9054.
- D.-I. Won, J.-S. Lee, Q. Ba, Y.-J. Cho, H.-Y. Cheong, S. Choi, C.H. Kim, H.-J. Son, C. Pac, S.O. Kang, Development of a Lower Energy Photosensitizer for Photocatalytic CO<sub>2</sub> Reduction: Modification of Porphyrin Dye in Hybrid Catalyst System, *ACS Catal.* 8 (2018) 1018–1030.
- R. Li, W. Zhang, K. Zhou, Metal–Organic–Framework-Based Catalysts for Photoreduction of CO<sub>2</sub>, *Adv. Mater.* 30 (2018) 1705512.
- H. Huang, J. Lin, G. Zhu, Y. Weng, X. Wang, X. Fu, J. Long, A Long-Lived Mononuclear Cyclopentadienyl Ruthenium Complex Grafted onto Anatase TiO<sub>2</sub> for Efficient CO<sub>2</sub> Photoreduction, *Angew. Chem., Int. Ed.* 55 (29) (2016) 8314–8318.
- B. Ma, G. Chen, C. Fave, L. Chen, R. Kuriki, K. Maeda, O. Ishitani, T.-C. Lau, J. Bonin, M. Robert, Efficient Visible-Light-Driven CO<sub>2</sub> Reduction by a Cobalt Molecular Catalyst Covalently Linked to Mesoporous Carbon Nitride, *J. Am. Chem. Soc.* 142 (2020) 6188–6195.
- K.E. Dalle, J. Warnan, J.J. Leung, B. Reuillard, I.S. Karmel, E. Reisner, Electro- and Solar-Driven Fuel Synthesis with First Row Transition Metal Complexes, *Chem. Rev.* 119 (4) (2019) 2752–2875.
- J.-D. Yi, R. Xu, G.-L. Chai, T. Zhang, K. Zang, B. Nan, H. Lin, Y.-L. Liang, J. Lv, J. Luo, R. Si, Y.-B. Huang, R. Cao, Cobalt Single-atoms Anchored on Porphyrinic Triazine-based Frameworks as Bifunctional Electrocatalysts for Oxygen Reduction and Hydrogen Evolution Reactions, *J. Mater. Chem. A* 7 (3) (2019) 1252–1259.
- A. Zitolo, N. Ranjbar-Sahraie, T. Mineva, J. Li, Q. Jia, S. Stamatini, G.F. Harrington, S.M. Lyth, S. Mukerjee, E. Honda, F. Jaouen, Identification of Catalytic Sites in Cobalt-Nitrogen-Carbon Materials for the Oxygen Reduction Reaction, *Nat. Commun.* 8 (2017) 957.
- X. Zhao, X. Liu, M. Yu, C. Wang, J. Li, The Highly Efficient and Stable Cu Co, Zn-porphyrin–TiO<sub>2</sub> Photocatalysts with Heterojunction by Using Fashioned One-step Method, *Dyes Pigm.* 136 (2017) 648–656.
- N. Ahmed, Y. Shibata, T. Taniguchi, Y. Izumi, Photocatalytic Conversion of Carbon Dioxide into Methanol Using Zinc–Copper–M(III) (M = Aluminum, Gallium) Layered Double Hydroxides, *J. Catal.* 279 (1) (2011) 123–135.
- H. Zhang, S. Kawamura, M. Tamba, T. Kojima, M. Yoshida, Y. Izumi, Is Water More Reactive Than H<sub>2</sub> in Photocatalytic CO<sub>2</sub> Conversion into Fuels Using Semiconductor Catalysts under High Reaction Pressures?, *J. Catal.* 352 (2017) 452–465.
- A.N. Marianov, A.S. Kochubei, T. Roman, O.J. Conquest, C. Stampfl, Y. Jiang, Resolving Deactivation Pathways of Co Porphyrin-Based Electrocatalysts for CO<sub>2</sub> Reduction in Aqueous Medium, *ACS Catal.* 11 (6) (2021) 3715–3729.
- S. Lin, C.S. Diercks, Y.-B. Zhang, N. Kornienko, E.M. Nichols, Y. Zhao, A.R. Paris, D. Kim, P. Yang, O.M. Yaghi, C.J. Chang, Covalent Organic Frameworks Comprising Cobalt Porphyrins for Catalytic CO<sub>2</sub> Reduction in Water, *Science* 349 (2015) 1208–1213.
- A.N. Marianov, Y. Jiang, Covalent Ligation of Co Molecular Catalyst to Carbon Cloth for Efficient Electroreduction of CO<sub>2</sub> in Water, *Appl. Catal. B* 244 (2019) 881–888.
- X.-M. Hu, M.H. Rønne, S.U. Pedersen, T. Skrydstrup, K. Daasbjerg, Enhanced Catalytic Activity of Cobalt Porphyrin in CO<sub>2</sub> Electroreduction upon Immobilization on Carbon Materials, *Angew. Chem. Int. Ed.* 56 (23) (2017) 6468–6472.
- C. Zheng, X. Qiu, J. Han, Y. Wu, S. Liu, Zero-Dimensional-g-CNQD-Coordinated Two-Dimensional Porphyrin MOF Hybrids for Boosting Photocatalytic CO<sub>2</sub> Reduction, *ACS Appl. Mater. Interfaces* 11 (45) (2019) 42243–42249.
- S. Tian, S. Chen, X. Ren, Y. Hu, H. Hu, J. Sun, F. Bai, An Efficient Visible-Light Photocatalyst for CO<sub>2</sub> Reduction Fabricated by Cobalt Porphyrin and Graphitic Carbon Nitride via Covalent Bonding, *Nano Resear.* 13 (10) (2020) 2665–2672.
- J. Xu, X. Liu, Z. Zhou, M. Xu, Photocatalytic CO<sub>2</sub> Reduction Catalyzed by Metalloporphyrin: Understanding of Cobalt and Nickel Sites in Activity and Adsorption, *Appl. Surf. Sci.* 513 (2020) 145801.
- J. Xu, X. Liu, Z. Zhou, L. Deng, L. Liu, M. Xu, Visible Light-Driven CO<sub>2</sub> Photocatalytic Reduction by Co-Porphyrin-Coupled MgAl Layered Double-Hydroxide Composite, *Energy Fuels* 35 (19) (2021) 16134–16143.
- N. Sadeghi, M. Sillanpää, High Selective Photocatalytic CO<sub>2</sub> Conversion into Liquid Solar Fuel over a Cobalt Porphyrin-Based Metal–Organic Framework, *Photochem. Photobiol. Sci.* 20 (3) (2021) 391–399.
- L. Wang, P. Jin, J. Huang, H. She, Q. Wang, Integration of Copper(II)-Porphyrin Zirconium Metal–Organic Framework and Titanium Dioxide to Construct Z-Scheme System for Highly Improved Photocatalytic CO<sub>2</sub> Reduction, *ACS Sustainable, Chem. Eng.* 7 (2019) 15660–15670.
- Y. Yoshida, Y. Mitani, T. Itoi, Y. Izumi, Preferential Oxidation of Carbon Monoxide in Hydrogen Using Zinc Oxide Photocatalysts Promoted and Tuned by Adsorbed Copper Ions, *J. Catal.* 287 (2012) 190–202.
- J.A. Bearden, X-Ray Wavelengths, *Rev. Modern Phys.* 39 (1) (1967) 78–124.
- F.W. Lytle, R.B. Gregor, D.R. Sandstrom, E.C. Marques, J. Wong, C.L. Spiro, G.P. Huffman, F.E. Huggins, Measurement of Soft X-Ray Absorption Spectra with a Fluorescent Ion Chamber Detector, *Nuclear Instrum. Meth. Phys. Resear.* 226 (1984) 542–548.
- M. Vaarkamp, H. Linders, D. Koningsberger, XDPAT Version 3.2.8, XAFS Services International, Woudenberg, The Netherlands, 2021.
- [https://www.webelements.com/cobalt/crystal\\_structure.html](https://www.webelements.com/cobalt/crystal_structure.html) (checked on February 27, 2022).
- W. Jauch, M. Reehuis, H.J. Bleif, F. Kubanek, P. Pattison, Crystallographic Symmetry and Magnetic Structure of CoO, *Phys. Rev. B* 64 (2001) 052102.
- M. J. Frisch, G. W. Trucks, H. B. Schlegel, G. E. Scuseria, M. A. Robb, J. R. Cheeseman, G. Scalmani, V. Barone, B. Mennucci, G. A. Petersson, H. Nakatsuji, et al. Gaussian 09, Revision A. 2, Gaussian, Inc., Wallingford CT, USA, 2016.
- H. Gao, J. Wang, M. Jia, F. Yang, R.S. Andriamitantsoa, X. Huang, W. Dong, G. Wang, Construction of TiO<sub>2</sub> Nanosheets/Tetra (4-Carboxyphenyl) Porphyrin Hybrids for Efficient Visible-light Photoreduction of CO<sub>2</sub>, *Chem. Eng. J.* 374 (2019) 684–693.
- S. Devaramani, M.I. Shinger, X. Ma, M. Yao, S. Zhang, D. Qin, X. Lu, Porphyrin Aggregates Decorated MWCNT Film for Solar Light Harvesting: Influence of J- and H-aggregation on the Charge Recombination Resistance, Photocatalysis, and Photoinduced Charge Transfer Kinetics, *Phys. Chem. Chem. Phys.* 19 (2017) 18232–18242.

- [36] E.H.A. Beckers, S.C.J. Meskers, A.P.H.J. Schenning, Z. Chen, F. Würthner, P. Marsal, D. Beljonne, J. Cornil, R.A.J. Janssen, Influence of Intermolecular Orientation on the Photoinduced Charge Transfer Kinetics in Self-Assembled Aggregates of Donor–Acceptor Arrays, *J. Am. Chem. Soc.* 128 (2) (2006) 649–657.
- [37] B. Zhuang, X.Q. Li, R.Y. Ge, S.Z. Kang, L.X. Qin, G.D. Li, Assembly and Electron Transfer Mechanisms on Visible Light Responsive 5,10,15,20-meso-tetra(4-Carboxyphenyl)Porphyrin/Cuprous Oxide Composite for Photocatalytic Hydrogen Production, *Appl. Catal. A* 533 (2017) 81–89.
- [38] Q. Xiang, J. Yu, M. Jaroniec, Enhanced Photocatalytic H<sub>2</sub>-Production Activity of Graphene-Modified Titania Nanosheets, *Nanoscale* 3 (2011) 3670–3678.
- [39] W. Hou, W.H. Hung, P. Pavaskar, A. Goepfert, M. Aykol, S.B. Cronin, Photoatalytic Conversion of CO<sub>2</sub> to Hydrocarbon Fuels via Plasmon-Enhanced Absorption and Metallic Interband Transitions, *ACS Catal.* 1 (2011) 929–936.
- [40] K. Maeda, Direct Splitting of Pure Water into Hydrogen and Oxygen Using Rutile Titania Powder as a Photocatalyst, *Chem. Commun.* 49 (2013) 8404–8406.
- [41] R. Li, Y. Weng, X. Zhou, X. Wang, Y. Mi, R. Chong, H. Han, C. Li, Achieving Overall Water Splitting Using Titanium Dioxide-Based Photocatalysts of Different Phases, *Energy Environ. Sci.* 8 (8) (2015) 2377–2382.
- [42] H. Shahroosvand, S. Zakavi, A. Sousaraei, M. Eskandari, Saddle-Shaped Porphyrins for Dye-Sensitized Solar Cells: New Insight into the Relationship between Nonplanarity and Photovoltaic Properties, *Phys. Chem. Chem. Phys.* 17 (2015) 6347–6358.
- [43] R. Giovannetti, The Use of Spectrophotometry UV–Vis for the Study of Porphyrins, *Macro Nano, Spectrosc.* 1 (2012) 87–108.
- [44] F. Koch, M. Kullmann, U. Selig, P. Nuernberger, D.C.G. Götz, G. Bringmann, T. Brixner, Coherent Two-dimensional Electronic Spectroscopy in the Soret Band of a Chiral Porphyrin Dimer, *New J. Phys.* 15 (2013) 025006.
- [45] J. Roales, J.M. Pedrosa, M.G. Guillén, T. Lopes-Costa, P. Castillero, A. Barranco, A. R. González-Elipe, Free-Base Carboxyphenyl Porphyrin Films Using a TiO<sub>2</sub> Columnar Matrix: Characterization and Application as NO<sub>2</sub> Sensors, *Sensors* 15 (2015) 11118–11132.
- [46] X. Guo, B. Guo, T. Shi, The Photochemical and Electrochemical Properties of Chiral Porphyrin Dimer and Self-aggregate Nanorods of Cobalt(II) Porphyrin Dimer, *Inorganica Chim. Acta* 363 (2010) 317–323.
- [47] J. Rochford, D. Chu, A. Hagfeldt, E. Galoppini, Tetrachelate Porphyrin Chromophores for Metal Oxide Semiconductor Sensitization: Effect of the Spacer Length and Anchoring Group Position, *J. Am. Chem. Soc.* 129 (2007) 4655–4665.
- [48] L. Mino, G. Spoto, A.M. Ferrari, CO<sub>2</sub> Capture by TiO<sub>2</sub> Anatase Surfaces: A Combined DFT and FTIR Study, *J. Phys. Chem. C* 118 (43) (2014) 25016–25026.
- [49] L.F. Liao, C.F. Lien, D.L. Shieh, M.T. Chen, J.L. Lin, FTIR Study of Adsorption and Photoassisted Oxygen Isotopic Exchange of Carbon Monoxide, Carbon Dioxide, Carbonate, and Formate on TiO<sub>2</sub>, *J. Phys. Chem. B* 106 (2002) 11240–11245.
- [50] U. Tumuluri, J.D. Howe, W.P. Mounfield, M. Li, M. Chi, Z.D. Hood, K.S. Walton, D.S. Sholl, S. Dai, Z. Wu, Effect of Surface Structure of TiO<sub>2</sub> Nanoparticles on CO<sub>2</sub> Adsorption and SO<sub>2</sub> Resistance, *ACS Sustainable Chem. Eng.* 5 (2017) 9295–9306.
- [51] M.-Y. He, J.G. Ekerdt, Infrared Studies of the Adsorption of Synthesis Gas on Zirconium Dioxide, *J. Catal.* 87 (1984) 381–388.
- [52] F. Huber, J. Berwanger, S. Polesya, S. Mankovsky, H. Ebert, F.J. Giessibl, Chemical Bond Formation Showing a Transition from Physisorption to Chemisorption, *Science* 366 (6462) (2019) 235–238.
- [53] N. Keller, M. Calik, D. Sharapa, H.R. Soni, P.M. Zehetmaier, S. Rager, F. Auras, A. C. Jakowetz, A. Görling, T. Clark, T. Bein, Enforcing Extended Porphyrin J-Aggregate Stacking in Covalent Organic Frameworks, *J. Am. Chem. Soc.* 140 (48) (2018) 16544–16552.
- [54] K.S. Min, R.S. Kumar, J.H. Lee, K.S. Kim, S.G. Lee, Y.-A. Son, Synthesis of new TiO<sub>2</sub>/porphyrin-based composites and photocatalytic studies on methylene blue degradation, *Dyes Pigments* 160 (2019) 37–47.
- [55] C. Liu, K. Liu, C. Wang, H. Liu, H. Wang, H. Su, X. Li, B. Chen, J. Jiang, Elucidating heterogeneous photocatalytic superiority of microporous porphyrin organic cage, *Nat. Commun.* 11 (2020) 1047.
- [56] D.-H. Won, J.-S. Lee, Q. Ba, Y.-J. Cho, H.-Y. Cheong, S. Choi, C. H. Kim, H.-J. Son, C. Pac, S. O. Kang, Development of a Lower Energy Photosensitizer for Photocatalytic CO<sub>2</sub> Reduction: Modification of Porphyrin Dye in Hybrid Catalyst System, *ACS Catal.* 8 (2018) 1018–1030.
- [57] T. Loumissi, K. Hara, H. Zhang, T. Oyumi, R. Ishii, R. Hirayama, K. Niki, T. Itoi, Y. Izumi, manuscript in preparation.